NASA TECHNICAL MEMORANDUM

NASA TM X-977

HYPERSONIC AERODYNAMIC CHARACTERISTICS OF FOUR SERIES OF BLUNT LIFTING BODY AND WINGED REENTRY CONFIGURATIONS

by Cuyler W. Brooks, Jr., and Charles D. Trescot, Jr.

Langley Research Center
Langley Station, Hampton, Va.

NATIONAL AERONAUTICS AND SPACE ADMINISTRATION   •   WASHINGTON, D. C.   •   JULY 1964

HYPERSONIC AERODYNAMIC CHARACTERISTICS OF FOUR SERIES OF

BLUNT LIFTING BODY AND WINGED REENTRY CONFIGURATIONS

By Cuyler W. Brooks, Jr., and Charles D. Trescot, Jr.

Langley Research Center
Langley Station, Hampton, Va.

NATIONAL AERONAUTICS AND SPACE ADMINISTRATION

HYPERSONIC AERODYNAMIC CHARACTERISTICS OF FOUR SERIES OF

BLUNT LIFTING BODY AND WINGED REENTRY CONFIGURATIONS*

By Cuyler W. Brooks, Jr., and Charles D. Trescot, Jr.
Langley Research Center

SUMMARY

l49??

Force and moment data have been obtained at a Mach number of 10.03 on four series of blunt lifting and winged bodies at angles of attack from $-30°$ to $30°$ at an angle of yaw of $0°$ and yaw angles from $-6°$ to $15°$ at an angle of attack of $0°$. The Reynolds number per foot was approximately 1.65×10^6. The models consisted of five conoidal bodies, eight flat-top conoidal bodies, three Clark-Y section delta-wing bodies, and two cone-flare bodies. The moment reference center was taken at 50-percent model length for all models.

The basic conoidal body was investigated with flattened areas on the top and sides of the aft portion and in a high-fineness-ratio version. The basic conoidal body was longitudinally and directionally stable except at angles of attack and yaw near $0°$. The flat areas had no significant aerodynamic effects. The high-fineness-ratio body was longitudinally and directionally stable about the moment reference center at 50 percent of the body length and had a maximum lift-drag ratio of 2.2, whereas the lift-drag ratio for the short conoidal body was 1.1.

Of the eight flat-top conoidal bodies, a delta-nose rectangular planform configuration had the largest maximum lift-drag ratio, 1.8. This model was longitudinally stable about the moment reference center. The nose and aft pitch controls on the basic flat-top conoidal body provided trim points at angles of attack from $-8°$ to $22°$ with control deflections from $0°$ to $30°$.

There was no significant aerodynamic effect due to use of vertical fins (except for a positive $6°$ shift in trim angle of attack) or rear upper-surface modifications on the longitudinal characteristics of the Clark-Y delta-wing body, which was longitudinally stable for all three configurations. The Clark-Y bodies were directionally unstable except for the body with vertical fins, which was directionally stable up to a yaw angle of $6°$.

Newtonian impact theory predictions were made of the longitudinal coefficients for some of the bodies tested. Generally fair agreement was obtained for values of lift and drag coefficients, but pitching-moment coefficient predictions were in poor agreement for some configurations.

---

*Title, Unclassified.

INTRODUCTION

The investigation reported herein was carried out in order to obtain data on the hypersonic aerodynamic characteristics of four series of configurations having widely differing reentry and recovery characteristics. The first two series consist of wingless lifting bodies, the third series consists of blunt delta-wing configurations, and the fourth series consists of ballistic cone-flare bodies. All models tested are part of a research program on reentry vehicles for military missions, as reported in references 1 and 2. The experimental data from the present investigation were previously included in reference 1. References 3 and 4 present data on the same configurations as the present investigation at Mach numbers of 5 and 8, respectively. Reference 5 presents data obtained at a Mach number of 18.5 on one configuration of the present investigation, and references 2 and 6 to 9 present the results of investigations of similar lifting bodies and thick wing configurations at Mach numbers up to 6.

The present investigation was conducted in the Langley 15-inch hypersonic flow apparatus at a Mach number of 10.03 and a Reynolds number per foot of approximately 1.65×10^6. Data were obtained over an angle-of-attack range of approximately $-30°$ to $30°$ at zero yaw and over an angle-of-yaw range of $-6°$ to $15°$ at an angle of attack of $0°$. In addition to determining the aerodynamic characteristics of the basic configurations of the four series, the effectiveness of nose and aft-mounted pitch controls on one configuration of the lifting-body series was also investigated.

SYMBOLS

Longitudinal force and moment coefficients are referred to the wind system of axes, and the lateral and directional force and moment coefficients are referred to the body system of axes. The moment reference center for each model is located as shown in figure 1. For all models, the longitudinal position of the moment reference center is at 50 percent of the total length. The force and pitching-moment coefficients are based on the model planform area and total length, and the rolling- and yawing-moment coefficients are based on the planform area and maximum span dimension, with the exception of models 4A and 4B. For these two models, the coefficients are based on the area of the forebody-cone base, the forebody-cone length (pitching moment), and the forebody-cone base diameter (rolling and yawing moment).

a_b vertical semiaxis of base reference ellipse (fig. 3)

a_n vertical semiaxis of nose reference ellipse (fig. 3)

b_b horizont██████ of base reference ellipse (fig. 3)

b_n horizontal semiaxis of nose reference ellipse (fig. 3)

b	reference span (not the same for all models; see table I)
$\bar{c}$	reference length (not the same for all models; see table I)
C_L	lift coefficient, $\dfrac{\text{Lift}}{q_\infty S}$
C_D	drag coefficient, $\dfrac{\text{Drag}}{q_\infty S}$
C_m	pitching-moment coefficient, $\dfrac{\text{Pitching moment}}{q_\infty S \bar{c}}$
C_l	rolling-moment coefficient, $\dfrac{\text{Rolling moment}}{q_\infty S b}$
C_n	yawing-moment coefficient, $\dfrac{\text{Yawing moment}}{q_\infty S b}$
C_Y	side-force coefficient, $\dfrac{\text{Side force}}{q_\infty S}$
L/D	lift-drag ratio, C_L/C_D
$(L/D)_{max}$	maximum lift-drag ratio
l	longitudinal distance between reference ellipses of conoidal models (fig. 3)
q_∞	free-stream dynamic pressure
R	radius
R_b	base radius of flat-top conoidal models
r	radial cylindrical coordinate (fig. 3)
S	reference area (not the same for all models; see table I)
x	longitudinal cylindrical coordinate (fig. 3)
x_{cp}	longitudinal center-of-pressure location
z_{cp}	vertical center-of-pressure location
α	angle of attack

δ_f flap deflection angle (fig. 1(e))

δ_n nose deflection angle (fig. 1(e))

θ angular cylindrical coordinate (fig. 3)

ψ angle of yaw

MODELS

Drawings of the models are presented in figure 1, and photographs are shown in figure 2. Four families or series of models were tested: the conoidal lifting bodies, the flat-top conoidal lifting bodies, the Clark-Y winged configurations, and the cone-flare bodies.

The conoidal series of models is designated by the numeral 1. (See figs. 1(a) and 1(b).) These configurations are composed of straight-line elements obtained by fairing between two reference ellipses located in parallel planes 12.95 inches apart. The major axes of the reference ellipses are rotated 90° with respect to one another. For configuration 1A, the forward portion of the basic form was removed and the end faired into a spheroidal nose. The total model length was 8.00 inches. Configurations 1B, 1C, and 1D were identical to configuration 1A, except for flat areas (referred to as "flats") located on the top and sides. Configuration 1B had a flat on top, configuration 1C had flats on the sides, and configuration 1D had flats on both the top and sides, as shown in figure 1(a). Configuration 1E consisted of the full basic form (12.95 inches between the reference ellipses), with a spheroidal nose faired into the forward reference ellipse. (See fig. 1(b).)

The second series of models is referred to as the flat-top conoidal series and is designated by the numeral 2. (See figs. 1(c), 1(d), 1(e), and 1(f).) The bodies all have plane top surfaces. The straight-line part of the bottom surface was obtained by fairing straight-line elements between the semicircular base and a reference line segment contained in the plane of the top surface and parallel to the plane of the base. For models 2A, 2B, 2C, 2F, and 2G, this reference line segment was shorter than the base diameter (the models were tapered); for the other models of this series (2D, 2E, and 2H), the reference line segment was equal to the base diameter. The noses of all these models were cylindrically rounded, all had sharp upper leading edges, and all had a total length of 9.90 inches, except for models 2C and 2H. These two models (figs. 1(c) and 1(f)) had rounded upper leading edges, and model 2H was 4.50 inches long with a curved nose of radius 2.25 inches. Configuration 2B differed from the basic flat-top conoidal configuration 2A only in that it had a boattail surface at the rear (fig. 1(c)). Configuration 2C was identical to configuration 2A except for the rounded upper leading edge (fig. 1(c)). Configurations 2D and 2E had a rectangular and a delta-nose planform, respectively (fig. 1(d)). Configuration 2F consisted of the basic flat-top conoidal model 2A with pitch-control flaps $\left(\delta_f = 15° \text{ and } 30°\right)$ on the aft lower surface. The windward surface of the flaps

is curved so as to conform to the body surface at $\delta_f = 0^\circ$. Configuration 2G consisted of model 2A with a deflectable nose $\left(\delta_n = 15^\circ \text{ and } 30^\circ\right)$ for pitch control (fig. 1(e)).

The winged-configuration series of models is designated by the numeral 3. (See figs. 1(g) and 1(h).) These models all had the same clipped-tip delta planform. The chordwise sections of models 3A and 3B were modified Clark-Y airfoil sections with flat lower surfaces, and model 3C had chordwise sections obtained from those of models 3A and 3B by extending the upper surface straight back from the point of maximum thickness to the base. Model 3A was provided with vertical fins; model 3B was identical except that it had no vertical fins.

The cone-flare series of models is designated by the numeral 4. (See fig. 1(i).) The two cone-flare models differed only in that the nose of model 4B had a 60° canted flat area.

APPARATUS AND TESTS

The present investigations were conducted in the Langley 15-inch hypersonic flow apparatus at a Mach number of 10.03 (an average over the test core), a total pressure of approximately 1000 lb/sq in. abs, a stagnation temperature of approximately 1400° F, and a Reynolds number per foot of approximately 1.65×10^6. The free-stream dynamic pressure q_∞ was approximately 1.7 lb/sq in. abs. The dynamic pressure q_∞ is computed from the Mach number 10.03 and the stagnation pressure. Details of the tunnel system are given in reference 10.

The models were base-mounted, and force and moment measurements were made by use of an internally located, water-cooled, six-component, strain-gage balance. In general, data were obtained for the configurations over an angle-of-attack range of -30° to 30° at a yaw angle of 0°. Because of tunnel-size limitations, however, model 1E was tested only up to an angle of attack of 20°. The negative angles of attack were obtained by inverting the model on the balance. The Clark-Y series was not tested at negative angles of attack. Data were obtained at yaw angles by rotating the model, balance, and sting 90° on the sting support, and all yaw data were obtained at an angle of attack of 0°. Each configuration was tested through an angle-of-yaw range from -6° to 15° with the exception of models 2D, 2E, 2F, and 2G, which were not tested in yaw.

The angle of attack and angle of yaw have been corrected for sting and balance deflections. The base pressure was measured during each run, and axial force was adjusted to the condition of free-stream static pressure at the base.

The possible errors in the force and moment data, based on an assumed balance accuracy of one-half of one percent of the balance load limits, are given in the following table:

Lift, lb . . . . ±0.5
Drag at 0° angle of attack, lb . . . . ±0.08
Drag at 30° angle of attack, lb . . . . ±0.3

Side force, lb . . . . ±0.1
Pitching moment, in-lb . . . . ±0.4
Rolling moment, in-lb . . . . ±0.1
Yawing moment, in-lb . . . . ±0.2

Because of the wide variation in model reference dimensions, the possible
errors are presented in terms of forces and moments. The model reference
dimensions are given in table I. The possible error in angle of attack α
is 0.1°.

THEORETICAL PREDICTIONS OF MODEL CHARACTERISTICS

Predictions of C_L, C_D, and C_m were made for a number of the models of
the present investigation by using simple Newtonian impact theory. No attempt
was made to account for the effects of skin friction. Coefficients were esti-
mated for models 1A, 1E, 2A, 2D, 2G, and 4A; for these models an exact or
closely approximate equation of the main part of the body surface was available.
For the models having spherical or nearly spherical noses, the contributions of
the nose portion to the total coefficients were obtained from reference 11.
The contributions of the cylindrical noses were calculated directly. The theo-
retical coefficient variations are shown on the data plots of the respective
models for comparison.

The singly curved or straight-line surfaces of models 1A and 1E are given
exactly by the equation

$$r = \frac{x}{l}\left[\frac{2a_b^2 b_b^2}{\left(a_b^2 + b_b^2\right) - \left(a_b^2 - b_b^2\right)\cos 2\theta}\right]^{1/2}$$

$$+ \left(1 - \frac{x}{l}\right)\left[\frac{2a_n^2 b_n^2}{\left(a_n^2 + b_n^2\right) - \left(a_n^2 - b_n^2\right)\cos 2\theta}\right]^{1/2} \tag{1}$$

where r, x, and θ are cylindrical coordinates with origin at the center of
the forward reference ellipse, l is the distance between the reference
ellipses, and a, b are the vertical and horizontal semiaxes, respectively,
of the base (subscript b) and nose (subscript n) reference ellipses. (See
fig. 3.) This equation was also used to approximate the bottom surfaces of
models 2A and 2D. For this purpose, the vertical semiaxis of the nose refer-
ence ellipse a_n is made arbitrarily small, so that the nose reference line is

replaced by an arbitrarily flat ellipse. Thus, the flat-top conoidal body shapes can be approached as closely as desired for calculation purposes. The value $a_n = 0.001 b_n$ was used in the present calculation. Since the bases of models 2A and 2D are semicircular, $a_b = b_b = R_b$ (R_b = 2 inches), and the first term on the right-hand side of equation (1) becomes $R_b \frac{x}{l}$. For model 2A, $b_n = 0.729$ inch, and for 2D, $b_n = 2.000$ inches.

Model 2G is identical to model 2A except for the deflected forward part of the body. This deflection is merely equivalent to an increased angle of attack of the forebody so far as calculations are concerned.

Model 4A is a simple cone-flare body with a spherical nose; calculations were made in the usual manner for the cone frustums comprising the configuration.

On all of the bodies to which equation (1) applies, the theoretical values of C_m for the models were calculated from the theoretical values of normal-force coefficient and the theoretical longitudinal center of pressure x_{cp} referenced to the moment center, plus the theoretical value of axial-force coefficient and an assumed value of z_{cp}. The theoretical value of x_{cp} for such surfaces is not easily calculated directly. The centers of pressure of the surfaces described by equation (1) can, however, be calculated for each elemental longitudinal strip on the surface, that is, for each value of θ. (See fig. 3.) If, as was true for some models, the theoretical location of the local center of pressure of an elemental strip as a function of θ varied only slightly with θ, then the location of the center of pressure on the lower surface line of symmetry ($\theta = \pi$) was used as the x_{cp} for the complete surface. For models where there was considerable variation of the local center of pressure with θ, a value of x_{cp} for the complete surface was selected by weighting the contributions of the elemental areas near $\theta = \pi$ more heavily, since the normal force is greatest in this region. The vertical location of center of pressure z_{cp} was assumed to be zero for the axially symmetric models (1A, 1E), and a value of $z_{cp} = \frac{1}{2} R_b = 1$ inch below the moment reference center was chosen for the flat-top models.

PRESENTATION OF RESULTS

The order of the figures presenting the experimental and theoretical results is as follows:

RESULTS AND DISCUSSION

Conoidal Bodies

Longitudinal characteristics.- The basic short conoidal body 1A, which is axially symmetrical (fig. 1(a)), is longitudinally stable through the angle-of-attack range except near $0°$, with the trim point at about $11°$. (See fig. 4(a).) $\left(\text{Since } \dfrac{\partial C_L}{\partial \alpha} \text{ is always positive for the present tests, } \dfrac{\partial C_m}{\partial \alpha} \text{ has the same sign as } \dfrac{\partial C_m}{\partial C_L}.\right)$ Configuration 1A has an $(L/D)_{max}$ of about 1.1 near an angle of attack of approximately $26°$.

Configurations 1B and 1D, tested to show the effect of a flat area on the rear upper surface of the short conoidal body, had essentially the same longitudinal characteristics as the basic body 1A except for a slight decrease in drag coefficient at negative angles of attack. (See fig. 4(a).) Configurations 1C and 1D, tested with symmetrically placed flat areas on the sides, had essentially the same longitudinal aerodynamic characteristics as the basic body and the body with the flat on the rear upper surface.

Increasing the fineness ratio of the basic conoidal configuration 1A to form configuration 1E caused slight increases in C_L and considerable decreases in C_D due to decreased bluntness. (See fig. 5(a).) The values of C_L and C_D are underpredicted by about 25 percent for configuration 1E by Newtonian impact theory, although the prediction for the basic body 2A is good below an angle of attack of about $20°$. The underprediction of minimum drag of the high-fineness-ratio configuration, compared to the good agreement of theory and experiment for the basic short conoidal body 1A, is thought to be due to the greater skin friction drag of configuration 1E. The high-fineness-ratio body 1E had an $(L/D)_{max}$ of about 2.2, twice that of the short conoidal body, at an angle of attack of approximately $11°$. It is interesting to note that the Newtonian impact theory prediction of lift-drag ratio is generally good for both bodies, although C_L and C_D are considerably underpredicted for configuration 1E.

At all test angles of attack, the high-fineness-ratio body 1E is longitudinally stable about the moment reference center at 50 percent of the total body length (fig. 5(a)). If, however, the pitching-moment coefficient for body 1E were referenced to a moment center 4 inches from the base (the same location as for body 1A), the higher fineness ratio body would be quite unstable throughout the angle-of-attack range. The stability characteristics of the short conoidal body 1A are well predicted at angles of attack above approximately $15°$; while for the higher fineness ratio body, stability was underpredicted at all angles of attack by about 40 percent, more than would be expected from the underprediction of C_L and C_D.

Lateral characteristics.- All of the short conoidal bodies (1A, 1B, 1C, and 1D) were directionally stable above a yaw angle of about 7°. (See fig. 4(b).) The only significant effect of the side flats (models 1C and 1D) on the lateral characteristics of the short conoidal body was a slight increase in directional instability in the unstable region below 7° yaw angle. The rear upper-surface flat had no effect on the lateral characteristics of the short conoidal body.

The high-fineness-ratio configuration 1E was directionally stable throughout the test yaw angle range and had about the same level of stability as the short conoidal body 1A at yaw angles above 10°. As noted for longitudinal stability, however, body 1E would be directionally unstable if the moment center were taken as being at 4 inches from the base as for body 1A.

Flat-Top Conoidal Bodies

Longitudinal characteristics.- The basic flat-top conoidal body 2A was, in general, longitudinally stable throughout the test angle-of-attack range, with one trim point at an angle of attack of approximately 9°. The $(L/D)_{max}$ was about 1.6 near an angle of attack of 13°, but L/D was still 1.5 at the trim angle of attack of 9°. (See fig. 6(a).)

Boattailing the basic flat-top conoidal body to produce configuration 2B caused large positive increments in C_m at positive angles of attack so that there was no trim point for this body in the test angle-of-attack range. Lift and drag coefficients were somewhat lower for the boattail body 2B than for the basic body 2A at positive angles of attack, but there was no significant effect on lift-drag ratio. As would be expected, there was essentially no effect of the boattail on the longitudinal characteristics at negative angles of attack. (See fig. 6(a).)

Rounding the upper leading edge of the basic flat-top conoidal body to form configuration 2C had essentially no effect on the longitudinal character-istics except for an increase in C_D.

The rectangular planform body 2D had no stable trim point in the test angle-of-attack range. (See fig. 7(a).) Compared to the basic body 2A (which has a tapered planform), body 2D had essentially the same values of C_L throughout the angle-of-attack range and considerable increases in C_D up to an angle of attack of about 14°, with a corresponding decrease in L/D. The delta-nose body 2E, which differed from body 2D only in the planform shape of the nose, had essentially the same longitudinal stability characteristics as the basic body 2A; and compared to body 2A, body 2E had a somewhat higher value of $(L/D)_{max}$ and L/D at trim (both about 1.8 for body 2E as against 1.6 for body 2A). (See fig. 7(a).)

The high-lift high-drag body 2H was longitudinally stable throughout the test angle-of-attack range with a trim point at about -11° angle of attack. It will be noted that, at this angle of attack, C_L and L/D were only very slightly positive for configuration 2H.

10

The Newtonian impact theory prediction of the longitudinal aerodynamic characteristics of the flat-top conoidal bodies 2A (tapered planform) and 2D (rectangular planform) is good except for the stability characteristics of configuration 2D. (See fig. 7(b).) The failure to predict C_m for the rectangular planform body is thought to be due to the fact that the shock wave does not conform to the body shape of configuration 2D as well as for the tapered planform body 2A, because of the wide nose of body 2D. This effect is most noticeable at the rear of the model, as can be seen in the schlieren photographs, figure 11(b).

The aft (body 2F) and nose (body 2G) pitch controls on the flat-top conoidal body 2A provide trim points at angles of attack from -8° ($\delta_f = 30^\circ$) to 22° ($\delta_n = 30^\circ$). (See fig. 8(a).) The aft pitch controls lose effectiveness at large negative angles of attack. At the trim point near -8° angle of attack, C_L and, therefore, L/D were zero. Lift coefficient was somewhat higher for the aft pitch-control bodies at positive angles of attack, and C_D was greater due to the use of pitch controls at angles of attack above about -4°. The aft pitch controls generally caused larger drag increases than the nose pitch controls. The effect on $(L/D)_{max}$ was a reduction from about 1.6 for the basic body 2A to about 1.4 for the 15° control deflections and to about 1.0 for the 30° control deflections.

The Newtonian impact theory prediction of the longitudinal aerodynamic characteristics of the basic flat-top conoidal body 2A and the $\delta_n = 15^\circ$ and 30° nose pitch-control bodies 2G (fig. 8(b)) is generally good except for the failure to predict the trim points and the region of unstable slope near an angle of attack of 0°. The failure of impact theory to predict C_m well for the deflected nose bodies is thought to be due to the failure of the theory to predict the variation of the center of pressure on the aft lower surface with angle of attack, since C_L is very nearly the same at a given angle of attack whether $\delta_n = 0^\circ$, 15°, or 30°. It can be seen in the schlieren photographs (fig. 11(d)) that since the shock wave pattern changes with angle of attack, the center of pressure on the portion of the lower surface aft of the deflected nose will probably not remain stationary throughout the angle-of-attack range.

Lateral characteristics.- All of the flat-top conoidal bodies investigated at yaw angles were directionally stable throughout the test yaw range. The boattail body 2B had slightly less directional stability than the basic body 2A, while the rounded-upper-leading-edge body 2C had essentially the same lateral characteristics as body 2A. (See fig. 6(b).) The high-lift high-drag body 2H had somewhat less directional stability than the basic body 2A throughout the test yaw range. (See fig. 7(c).)

Delta-Winged Configurations

Longitudinal characteristics.- The Clark-Y airfoil section delta-winged configurations were all longitudinally stable in the test angle-of-attack range.

The removal of the vertical fins caused a shift in the trim point from approximately 6° angle of attack to near 0°, and caused a slight reduction in drag. The $(L/D)_{max}$ was about 1.6 near an angle of attack of approximately 20° for all three configurations. (See fig. 9(a).)

Lateral characteristics.- The Clark-Y body with vertical fins 3A was directionally stable only below a yaw angle of 6°. The other two bodies, 3B and 3C, were directionally unstable throughout the test angle-of-yaw range. (See fig. 9(b).) As would be expected, the level of directional stability varies as the amount of side area behind the moment reference center: the body with vertical fins 3A is the most stable at all angles of yaw and body 3C, with the rear upper surface modification, is somewhat more stable than body 3B.

Cone-Flare Bodies

Longitudinal characteristics.- The cone-flare body 4A is a ballistic configuration with longitudinal stability throughout the angle-of-attack range. The canted-nose configuration 4B had essentially the same longitudinal stability as configuration 4A, but had the trim point at an angle of attack of approximately 2° instead of 0°. The $(L/D)_{max}$ of both cone-flare bodies was about 0.8. (See fig. 10(a).)

The Newtonian impact theory prediction of the longitudinal characteristics of the cone-flare body 4A is generally good. Impact theory cannot predict the sharp break in the C_m curve at an angle of attack of 9°, which is due to the bow shock impinging on the flare. (See schlieren photographs, fig. 11(f).)

Lateral characteristics.- Both cone-flare bodies were directionally stable throughout the test yaw range. (See fig. 10(b).) The canted-nose body 4B was considerably more stable than body 4A. The break in the yawing-moment curve at an angle of yaw of 9° results from the previously mentioned impingement of the bow shock on the cone flare.

SUMMARY OF RESULTS

An investigation has been conducted in the Langley 15-inch hypersonic flow apparatus at a Mach number of 10.03 on four series of lifting and winged bodies suitable for atmospheric reentry. Force and moment data were obtained at angles of attack from -30° to 30° for a yaw angle of 0° and at yaw angles from -6° to 15° at an angle of attack of 0°. The Reynolds number per foot was approximately 1.65×10^6.

The most significant results may be summarized as follows:

1. The short conoidal bodies were longitudinally and directionally stable except near angles of attack and yaw near 0°. Flat areas on the rounded aft surface of the short conoidal body had no significant effect on either the longitudinal or lateral aerodynamic characteristics.

2. The high-fineness-ratio conoidal body had a value of maximum lift-drag ratio $(L/D)_{max}$ of about 2.2 as compared with 1.1 for the basic conoidal body.

3. Of the flat-top conoidal bodies, the rectangular planform configuration with the delta nose had the highest $(L/D)_{max}$, 1.8. For the present moment reference center, this body was longitudinally stable from -30° to 30° angle of attack, although the rectangular planform body with the plain nose was not.

4. The nose and aft pitch controls on the basic flat-top conoidal body provided trim capability at angles of attack from -8° to 22°.

5. There was no significant effect of the vertical fins (except for a positive 6° shift in trim angle of attack) or rear upper surface modification on the longitudinal aerodynamic characteristics of the Clark-Y winged body, which is longitudinally stable at all angles of attack. These bodies were directionally unstable except for the body with the vertical fins which was stable up to a yaw angle of 6°.

6. The Newtonian impact theory predictions were generally in fair agreement for the lift and drag coefficients, but the pitching-moment coefficient predictions were in poor agreement for some configurations.

Langley Research Center,
    National Aeronautics and Space Administration,
        Langley Station, Hampton, Va., March 10, 1964.

REFERENCES

1. Sullivan, Phillip J., and Onspaugh, Carl M.: Analytical and Experimental Investigation of Hypersonic Lifting Re-Entry Vehicles - Pt. I. Experimental Phase. Vol. 3 - Mach Numbers 10 and 18.6. ASD-TDR-62-789, Pt. I, Vol. 3, U.S. Air Force, May 1963.

2. Rockhold, Vernon G., Onspaugh, Carl M., and Marcy, William L.: Study To Determine Aerodynamic Characteristics on Hypersonic Re-Entry Configurations. Pt. I - Experimental Phase. Vol. 2 - Experimental Report - Mach Number 5. WADD Tech. Rep. 61-56, Pt. I, Vol. 2, U.S. Air Force, Mar. 1961.

3. Onspaugh, Carl M., and Sullivan, Phillip J.: Analytical and Experimental Investigation of Hypersonic Lifting Re-Entry Vehicles - Pt. I. Experimental Phase. Vol. 1 - Mach Number 5. ASD-TDR-62-789, Pt. I, Vol. 1, U.S. Air Force, May 1963.

4. Onspaugh, Carl M., and Sullivan, Phillip J.: Analytical and Experimental Investigation of Hypersonic Lifting Re-Entry Vehicles - Pt. I. Experimental Phase. Vol. 2 - Mach Number 8. ASD-TDR-62-789, Pt. I, Vol. 2, U.S. Air Force, May 1963.

5. Shelton, P. C.: Force Data on a Blunt Body of Elliptical Cross Section. AEDC-TDR-62-153, 1962.

6. Wornom, Dewey E., and Olstad, Walter B.: Static Longitudinal Aerodynamic Characteristics of a Right Triangular Pyramidal Lifting Reentry Configuration at Mach Numbers of 3.00, 4.50, and 6.00 for Angles of Attack up to 56°. NASA TM X-675, 1962.

7. Rakich, John V.: Aerodynamic Performance and Static-Stability Characteristics of a Blunt-Nosed, Boattailed, 13° Half-Cone at Mach Numbers From 0.6 to 5.0. NASA TM X-570, 1961.

8. McDevitt, John B., and Rakich, John V.: The Aerodynamic Characteristics of Several Thick Delta Wings at Mach Numbers to 6 and Angles of Attack to 50°. NASA TM X-162, 1960.

9. Mayo, Edward E.: Static Control Characteristics of a Glider Reentry Configuration Having 79.5° Sweepback and 45° Dihedral at a Mach Number of 6.01. NASA TM X-538, 1961.

10. Putnam, Lawrence E., and Brooks, Cuyler W., Jr.: Static Longitudinal Aerodynamic Characteristics at a Mach Number of 10.03 of Low-Aspect-Ratio Wing-Body Configurations Suitable for Reentry. NASA TM X-733, 1962.

11. Wells, William R., and Armstrong, William O.: Tables of Aerodynamic Coefficients Obtained From Developed Newtonian Expressions for Complete and Partial Conic and Spheric Bodies at Combined Angles of Attack and Sideslip With Some Comparisons With Hypersonic Experimental Data. NASA TR R-127, 1962.

TABLE I.- MODEL REFERENCE DIMENSIONS

Designation	S, sq in.	$\bar{c}$, in.	b, in.
Conoidal bodies			
1A	17.170	8.000	2.954
1B	17.170	8.000	2.954
1C	17.018	8.000	2.830
1D	17.018	8.000	2.830
1E	22.072	13.477	2.954
Flat-top conoidal bodies			
2A	29.554	9.900	4.000
2B	29.554	9.900	4.000
2C	29.554	9.900	4.000
2D	38.837	9.900	4.000
2E	33.946	9.900	4.000
2F	29.554	9.900	4.000
2G	29.554	9.900	4.000
2H	18.077	4.500	4.500
Delta-winged bodies			
3A	25.573	8.890	4.450
3B	25.573	8.890	4.450
3C	25.573	8.890	4.450
Cone-flare bodies			
4A	3.833	4.970	2.209
4B	3.833	4.970	2.209

12.953

2.461

Moment reference center

.769 R

Outline of configuration 1E for comparison.

A

A

0.740

2.954

2.004

0.062 typ.

4.000

Section A-A: Reference ellipse

Top view

Outline of configuration 1E for comparison.

.615 R

5.050

0.578

2.018

8.000

Side view

Note 1. Configuration 1A is solid outline with no flats.

Note 2. Configuration 1B has a 5.050-inch flat on the aft upper surface.

Note 3. Configuration 1C has a 2.461-inch flat on each side at the rear.

Note 4. Configuration 1D has both aft upper surface and side flats.

(a) Conoidal configurations 1A, 1B, 1C, and 1D.

12.953

0.179 R

A

A

0.428

0.638

Section A-A: Reference ellipse

2.954

6.738

Top view

2.018

0.308 R

2.018

13.477

Side view
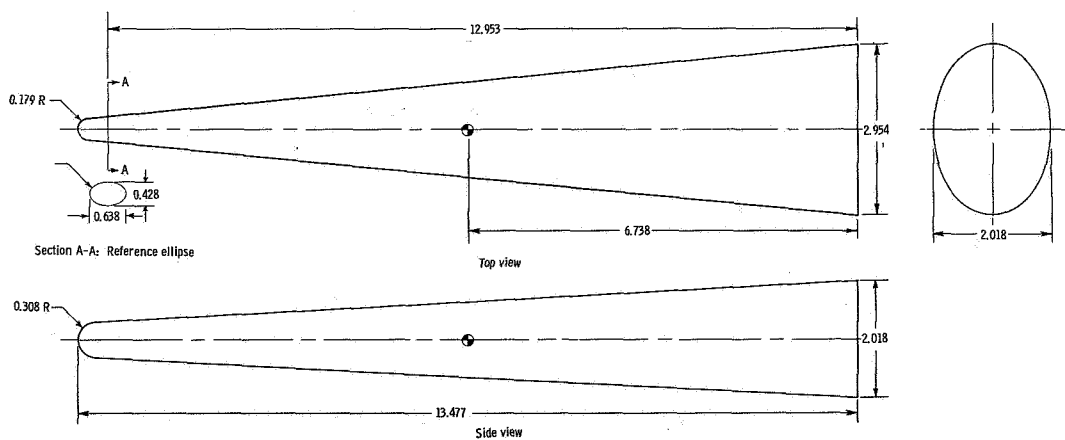
(b) Conoidal configuration 1E.

Figure 1.- Drawings of model configurations (design dimensions). All dimensions are in inches.

See Note 1.

12.587

0.67 R

4.000

4.950

9.900

1.150
See Note 2.

See Note 1.

0.50 R

2.000 R

Upper leading-edge radius is 0.120 on configuration 2C;
sharp (0.01) on 2A and 2B. This is the only difference
between 2A and 2C.

3.300
See Note 2.

2. Configuration 2B has 3.300-inch boattail on aft
lower surface.
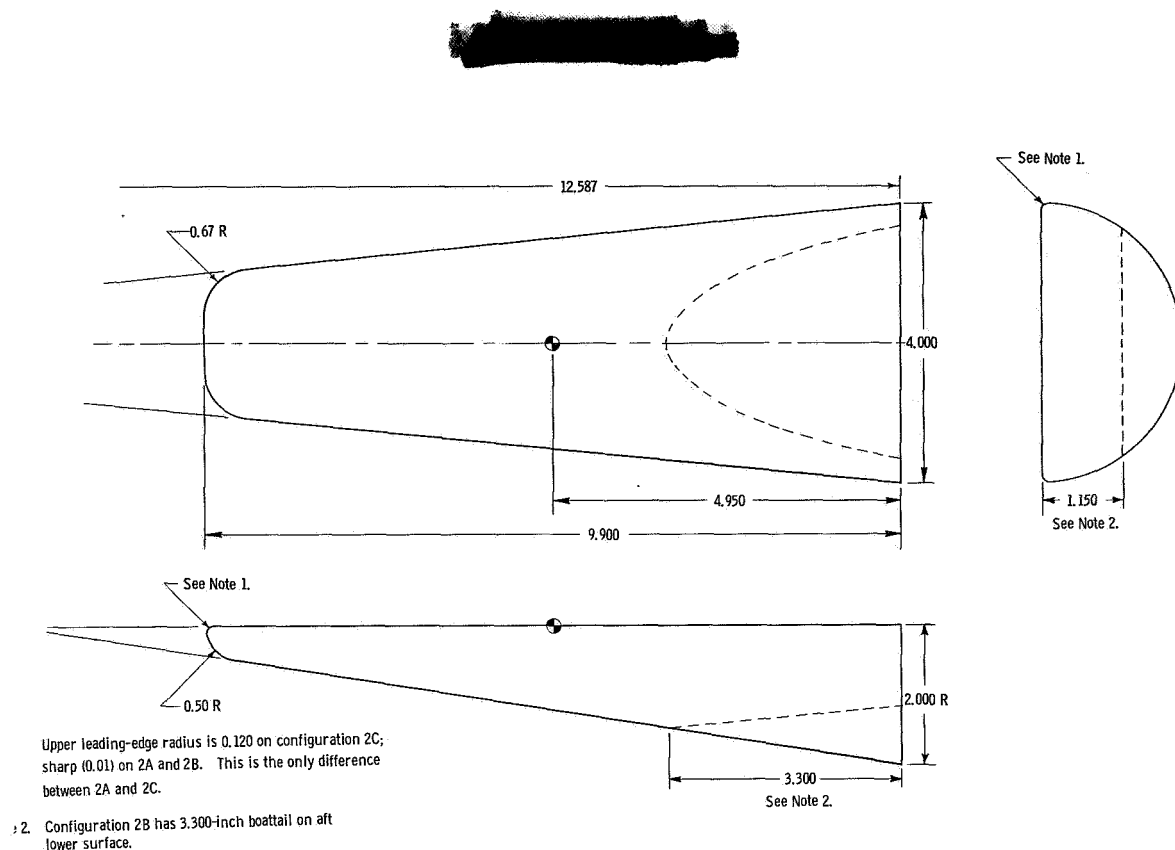
(c) Flat-top conoidal configurations 2A, 2B (boattail), and 2C (rounded upper leading edge).

6.600

4.950

4.000

54.407° 2E (delta nose)

0.50 R

1.34 R

9.900

0.50 R

2.000 R

12.587
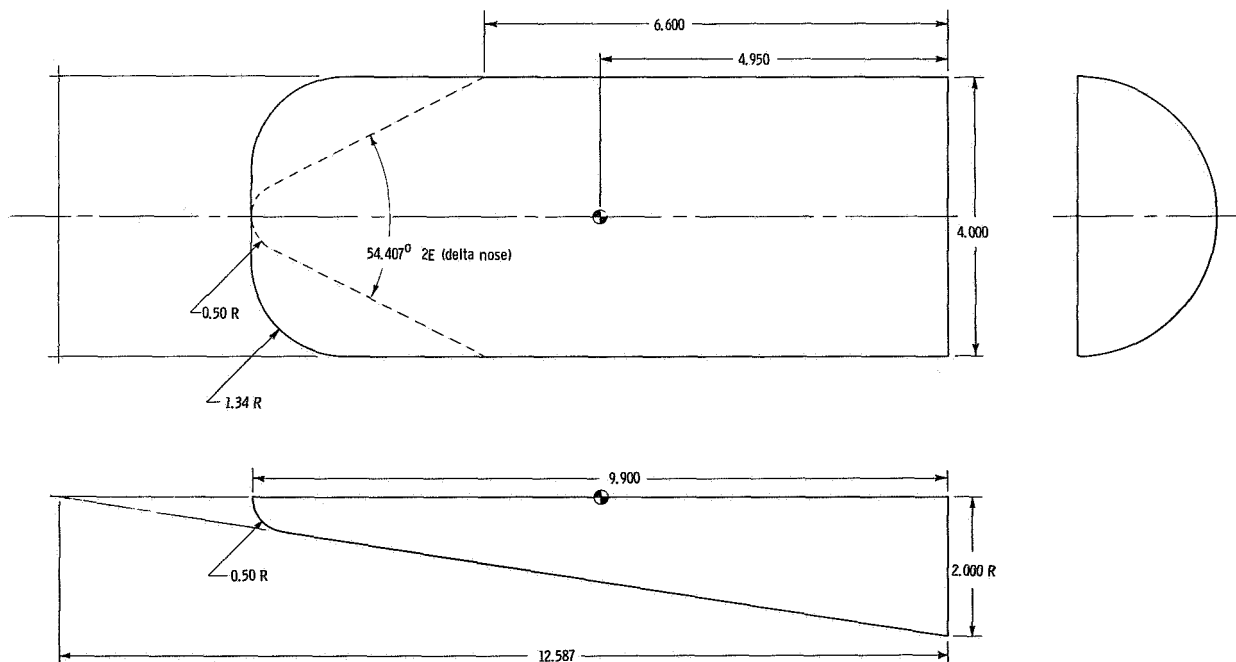
(d) Flat-top conoidal configurations 2D (rectangular planform) and 2E (delta nose).

Figure 1.- Continued.
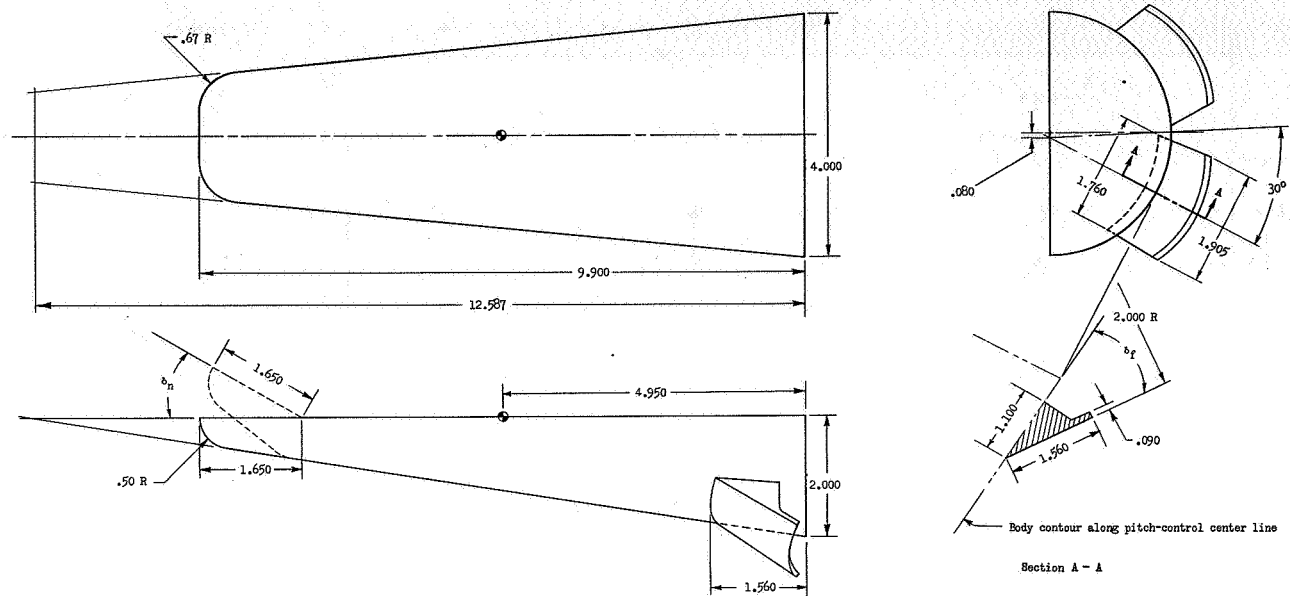
(e) Drawing showing aft pitch-control configuration 2F, $\delta_f = 15^\circ$ and 30°; forward pitch-control configuration 2G, $\delta_n = 15^\circ$ and 30°.
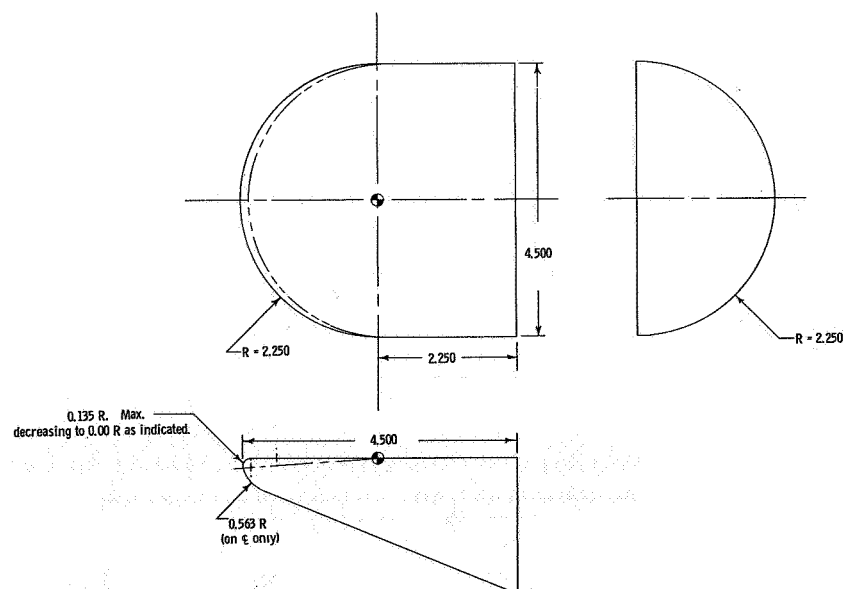
(f) Drawing of high-lift, high-drag configuration 2H.

Figure 1.- Continued.

Note: Configuration 3B is identical to 3A except that the vertical tails are off.
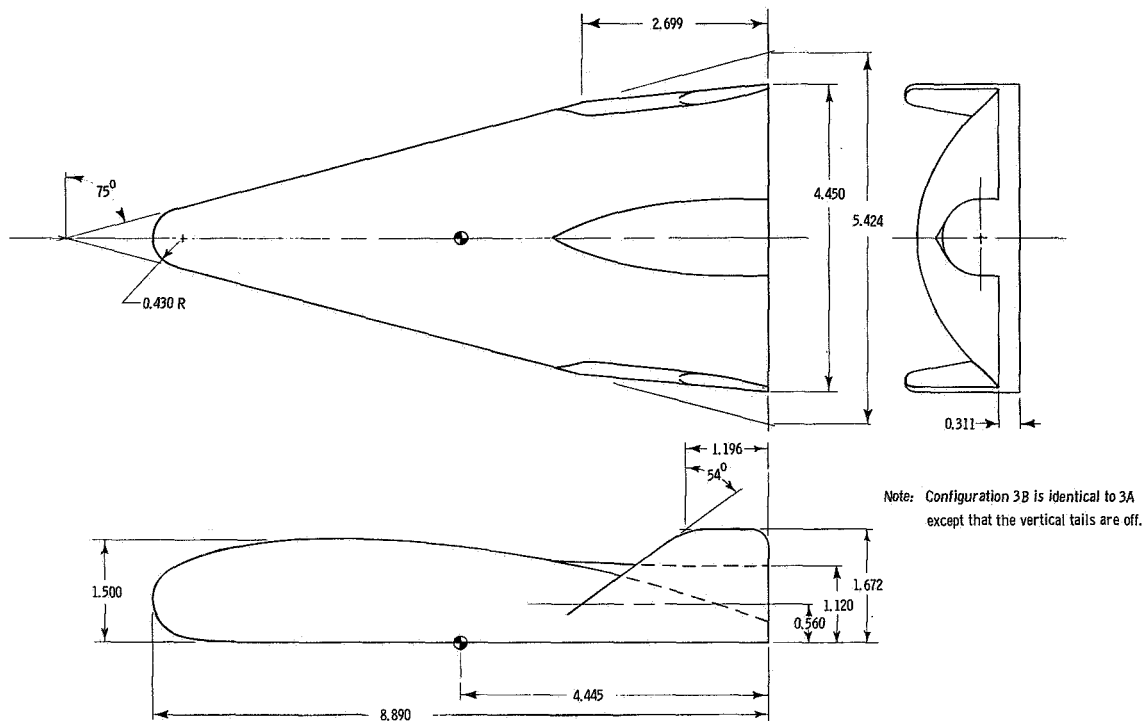
(g) Winged configurations 3A and 3B.
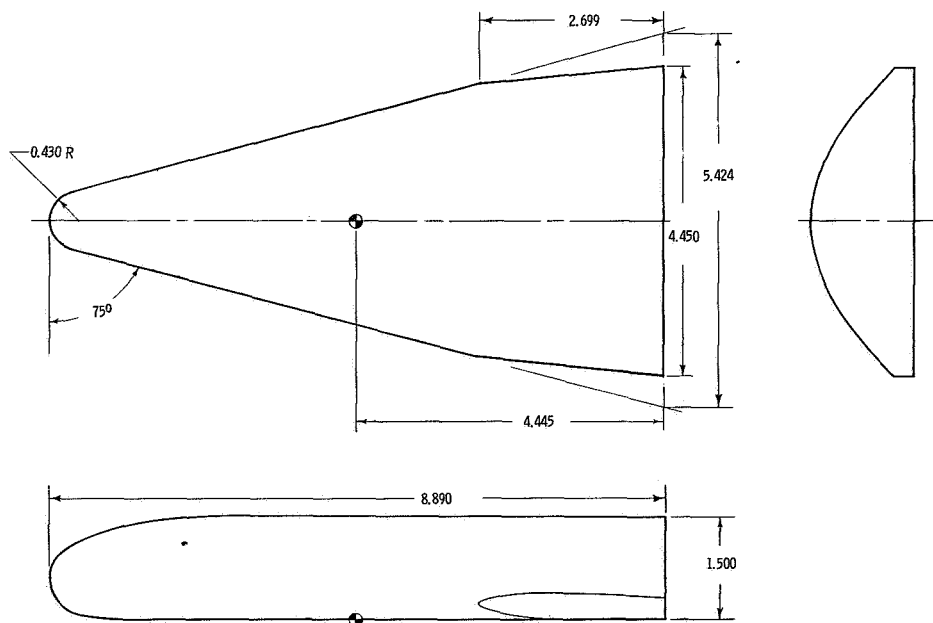
(h) Winged configuration 3C.

Figure 1.- Continued.

Top view

7.179

4.970

2.209

2.209

4.000

0.552
Spherical rad.

R = 2.000

3.590

60° Canted nose
model 4B

0.276 R

Side view
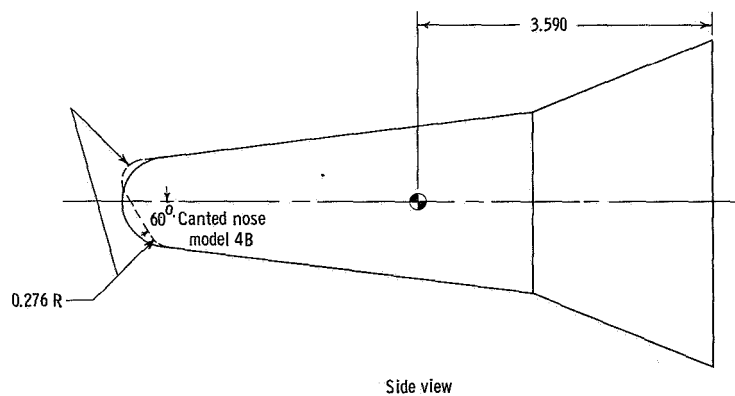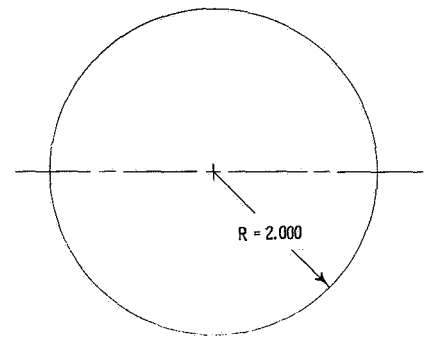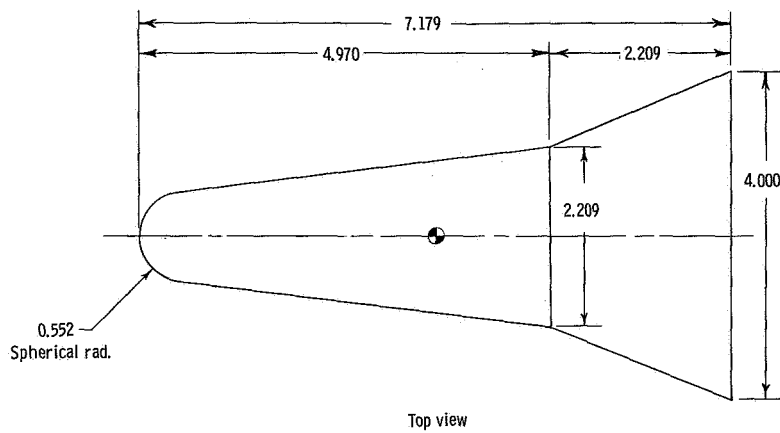
(i) Cone-flare configurations 4A and 4B.

Figure 1.- Concluded.
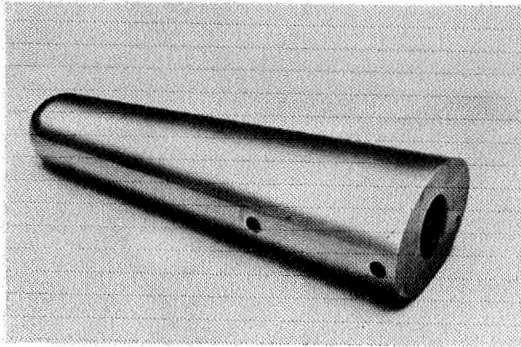
Model 1A
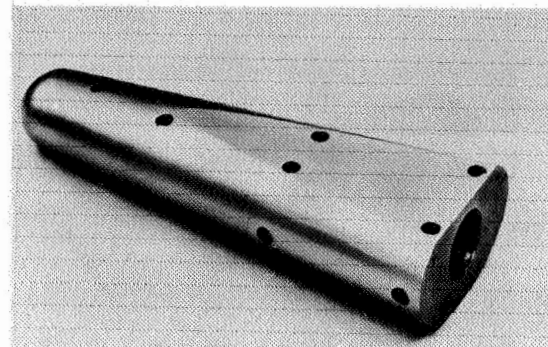
Model 1B
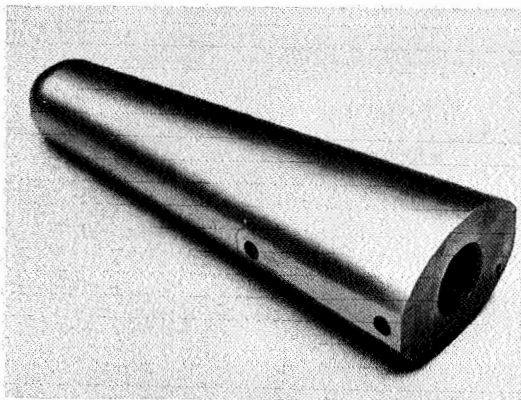
Model 1C
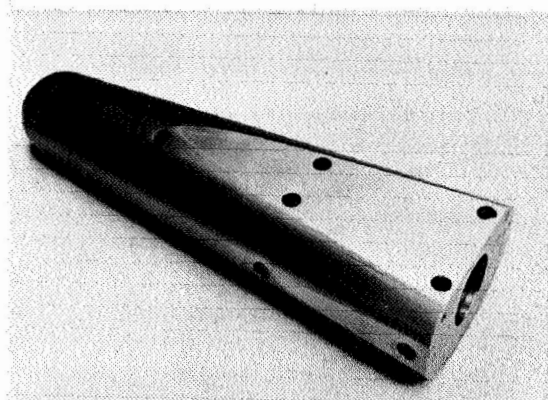
Model 1D
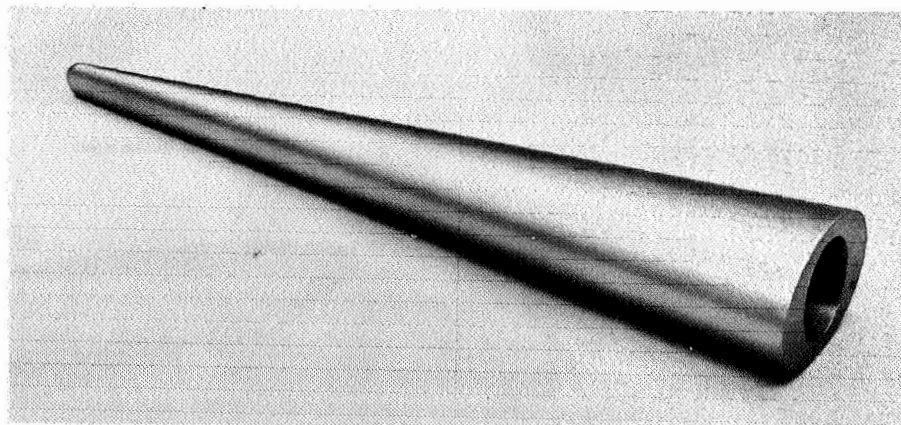
Model 1E

(a) Conoidal models.

L-64-432

Figure 2.- Photographs of models.
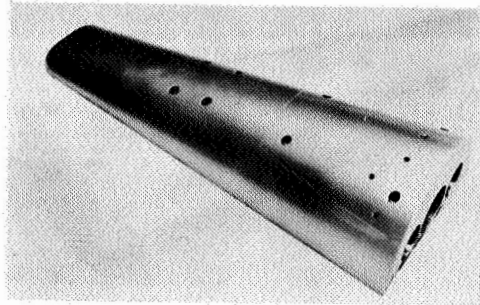
Model 2A (bottom view)
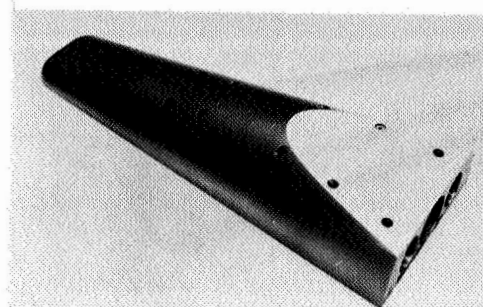
Model 2B (bottom view)
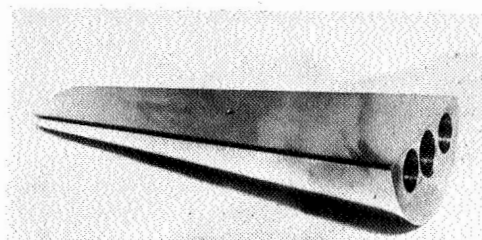
Model 2C (top view)
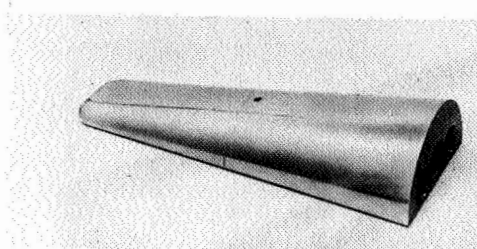
Model 2C (bottom view)
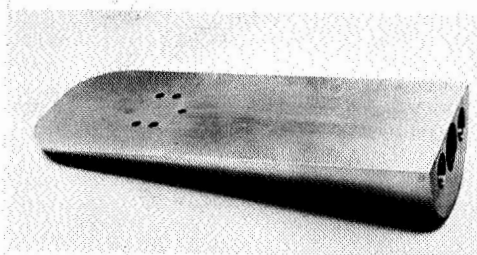
Model 2D (top view)
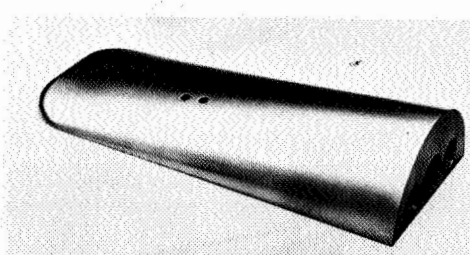
Model 2D (bottom view)
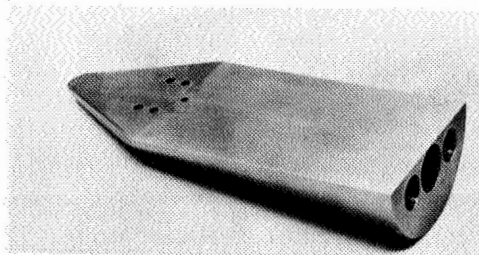
Model 2E (top view)
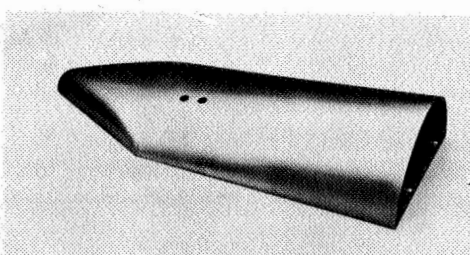
Model 2E (bottom view)

(b) Flat-top conoidal models.

L-64-433

Figure 2.- Continued.
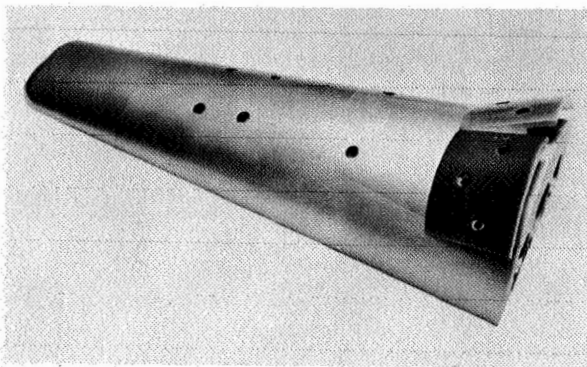
Model 2F, $\delta_f = 15^o$
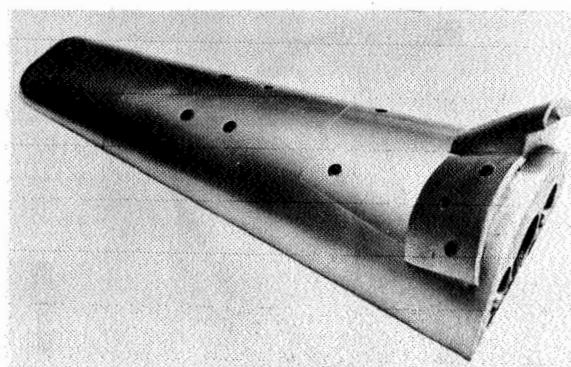
Model 2F, $\delta_f = 30^o$
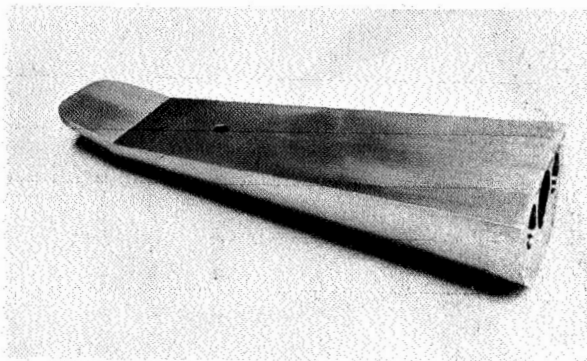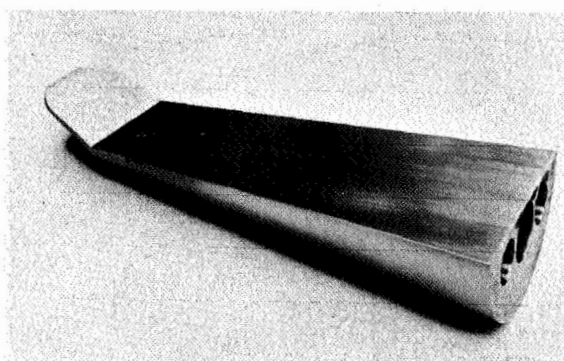
Model 2G, $\delta_n = 15^o$

Model 2G, $\delta_n = 30^o$

(c) Fore and aft pitch-control models.
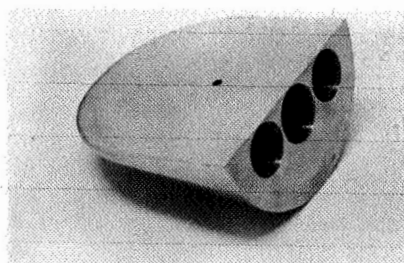
Model 2H (top view)
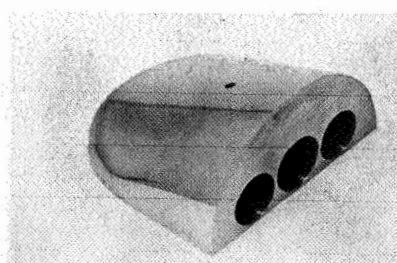
'Model 2H (bottom view)

(d) High-lift, high-drag model 2H.   L-64-434

Figure 2.- Continued.
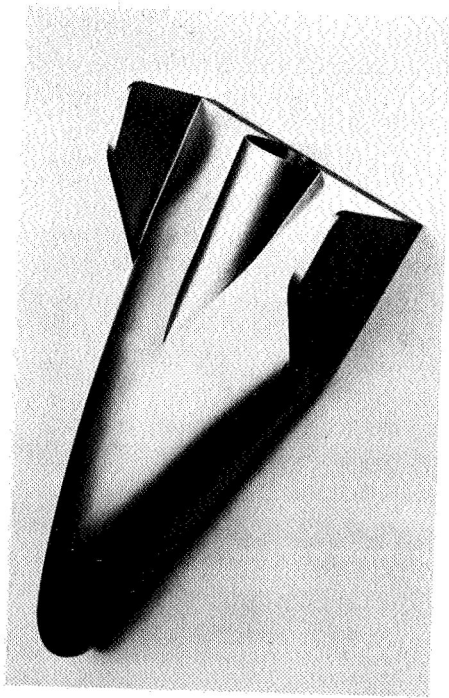
Model 3B
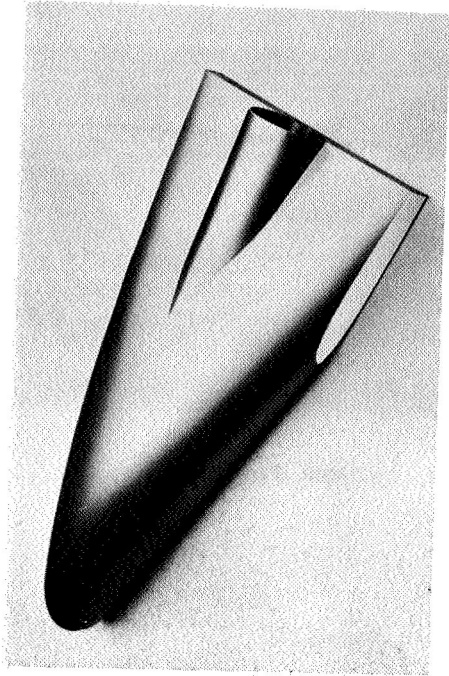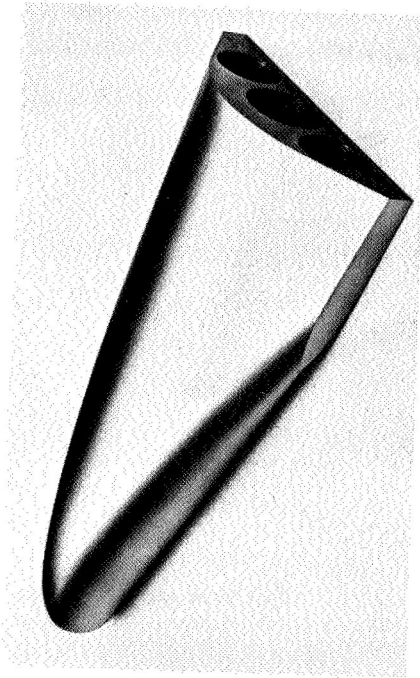
Model 3A

Model 3C

(e) Clark-Y models.

Figure 2.- Continued.

L-64-435

24
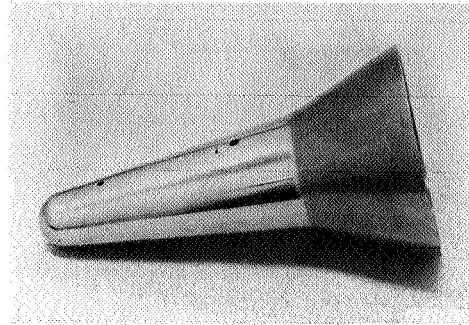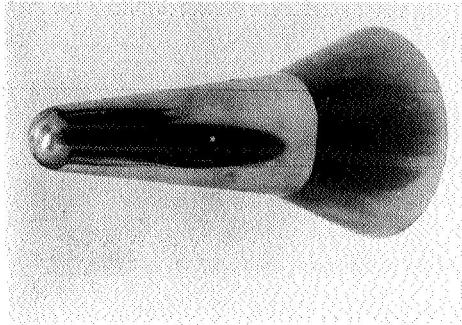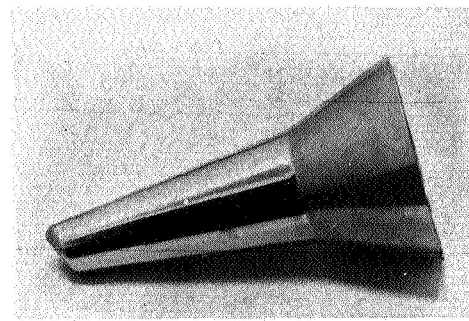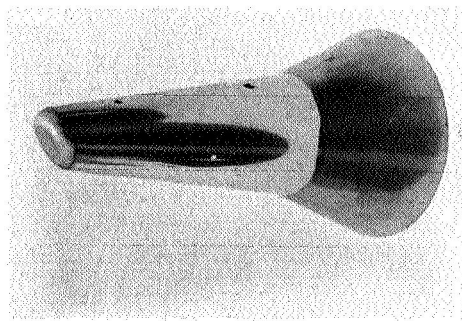
Model 4A

Model 4B

(f) Cone-flare models.

L-64-436

Figure 2.- Concluded.
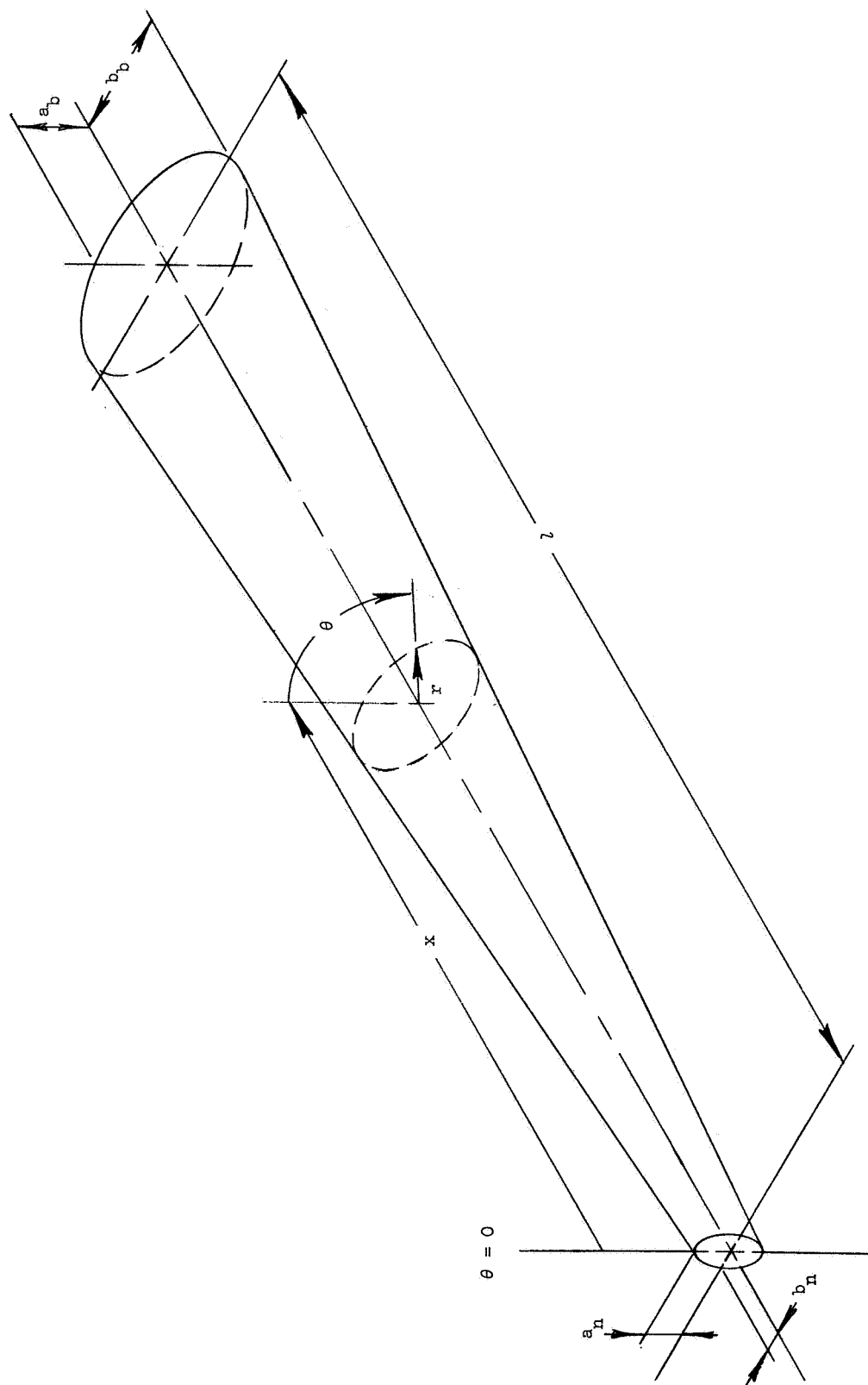
Figure 3.- Sketch of typical conoidal shape showing cylindrical coordinates.
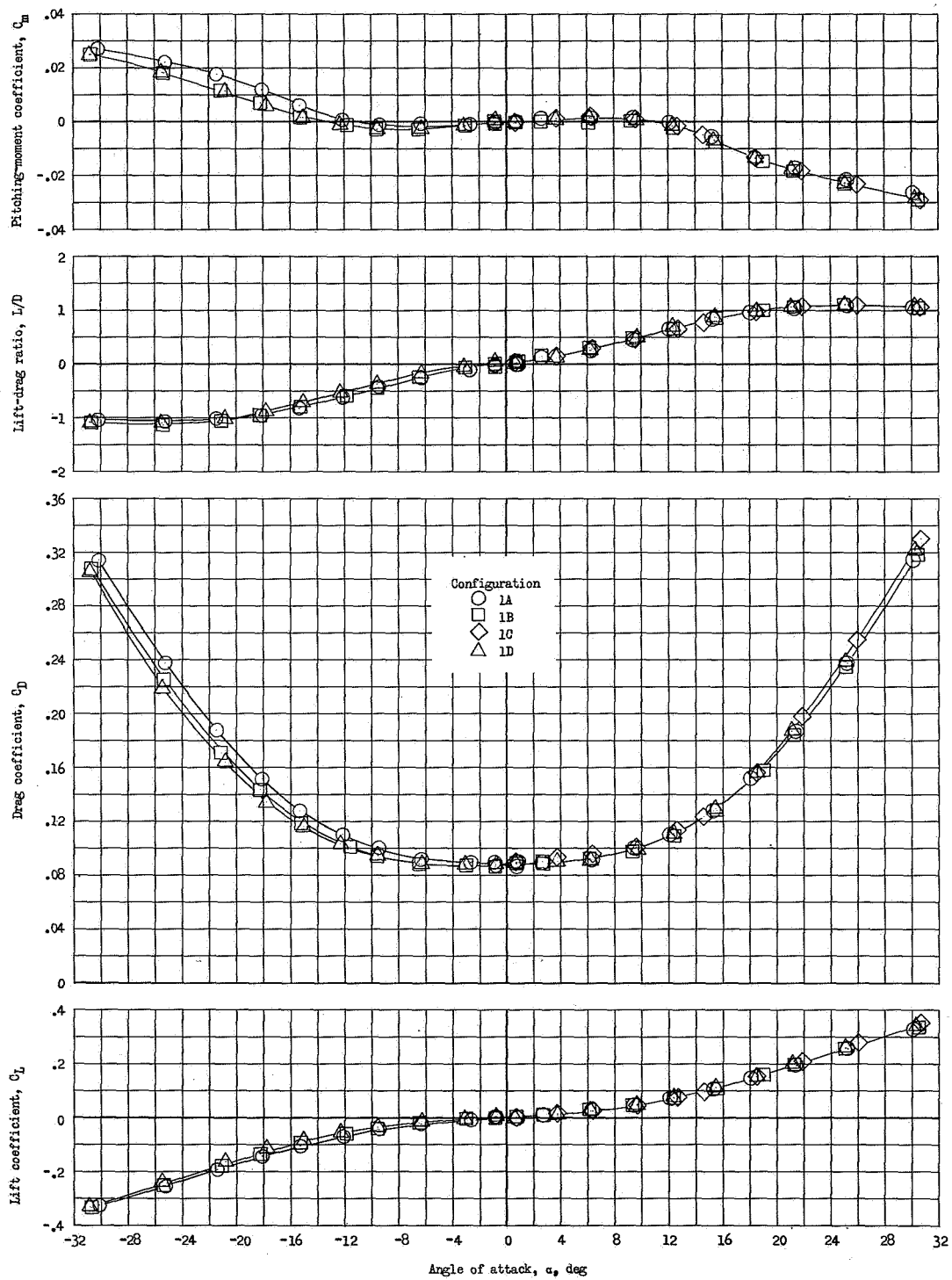
(a) Longitudinal characteristics.

Figure 4.- Effect of flat areas on aerodynamic characteristics of short conoidal models.
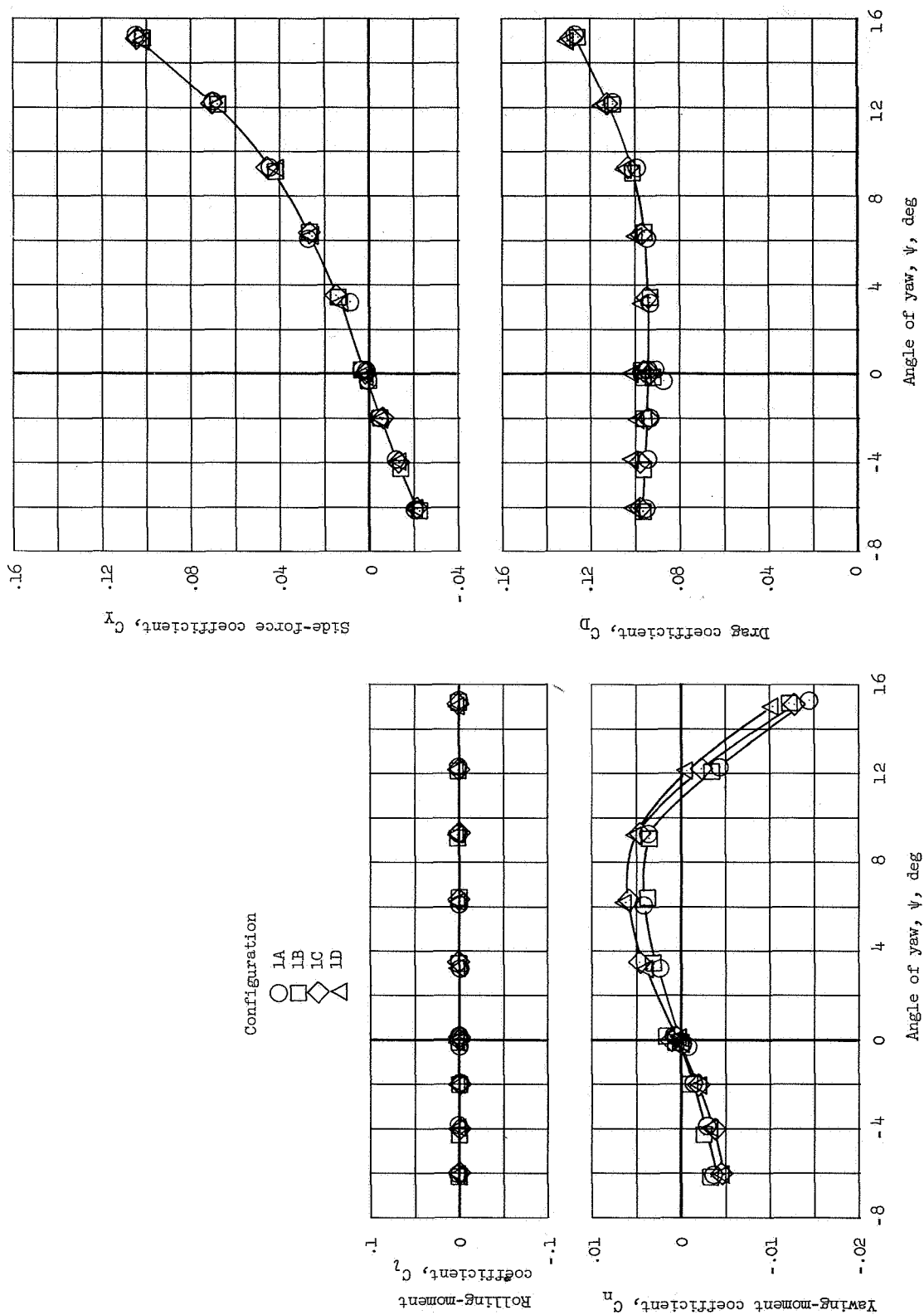
(b) Lateral characteristics.

Figure 4.- Concluded.
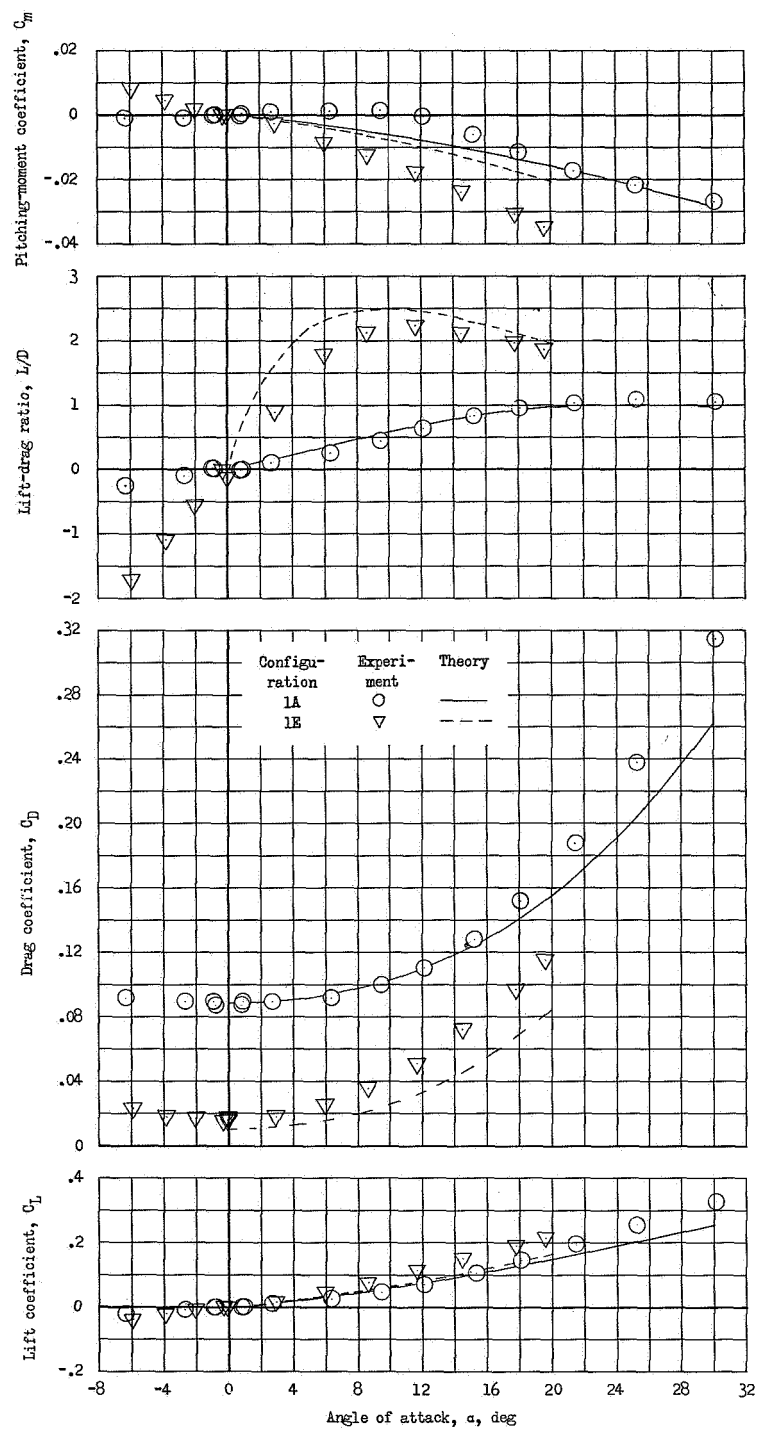
(a) Longitudinal data and Newtonian impact theory.

Figure 5.- Effect of fineness ratio on aerodynamic characteristics of basic conoidal model 1A.
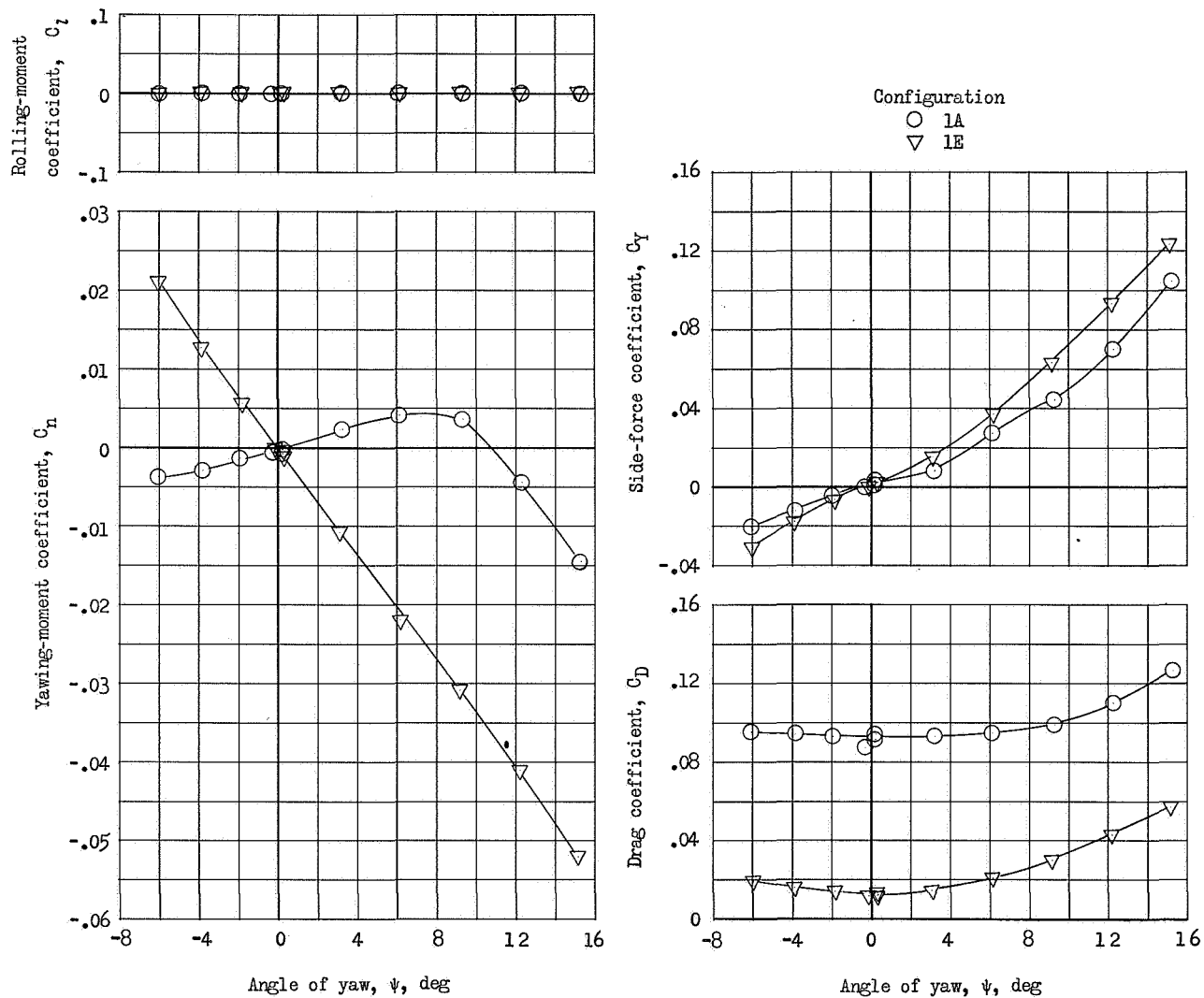
(b) Lateral characteristics.

Figure 5.- Concluded.
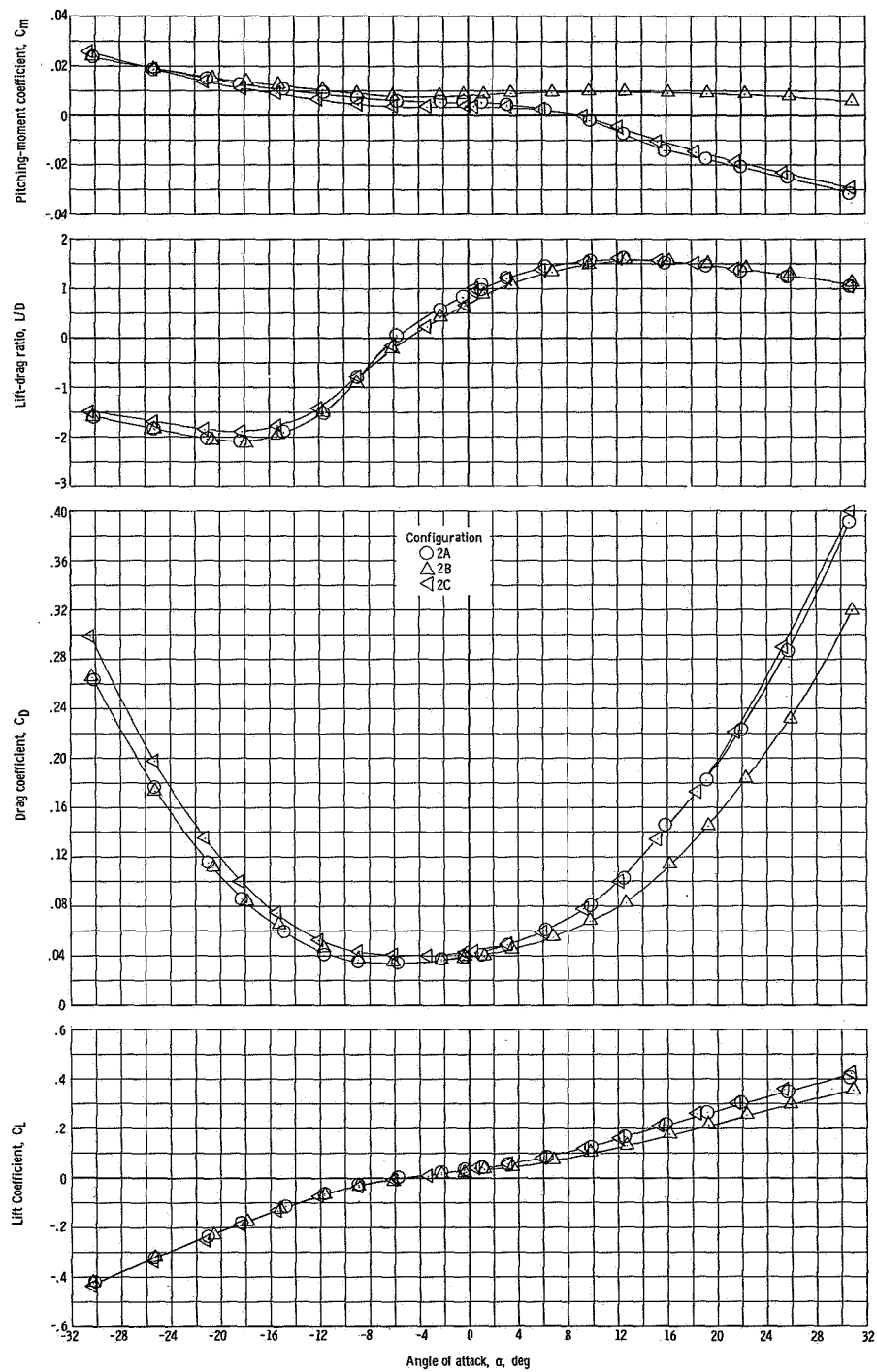
(a) Longitudinal characteristics.

Figure 6.- Effect of upper-leading-edge shape and boattail on characteristics of basic flat-top conoidal body.
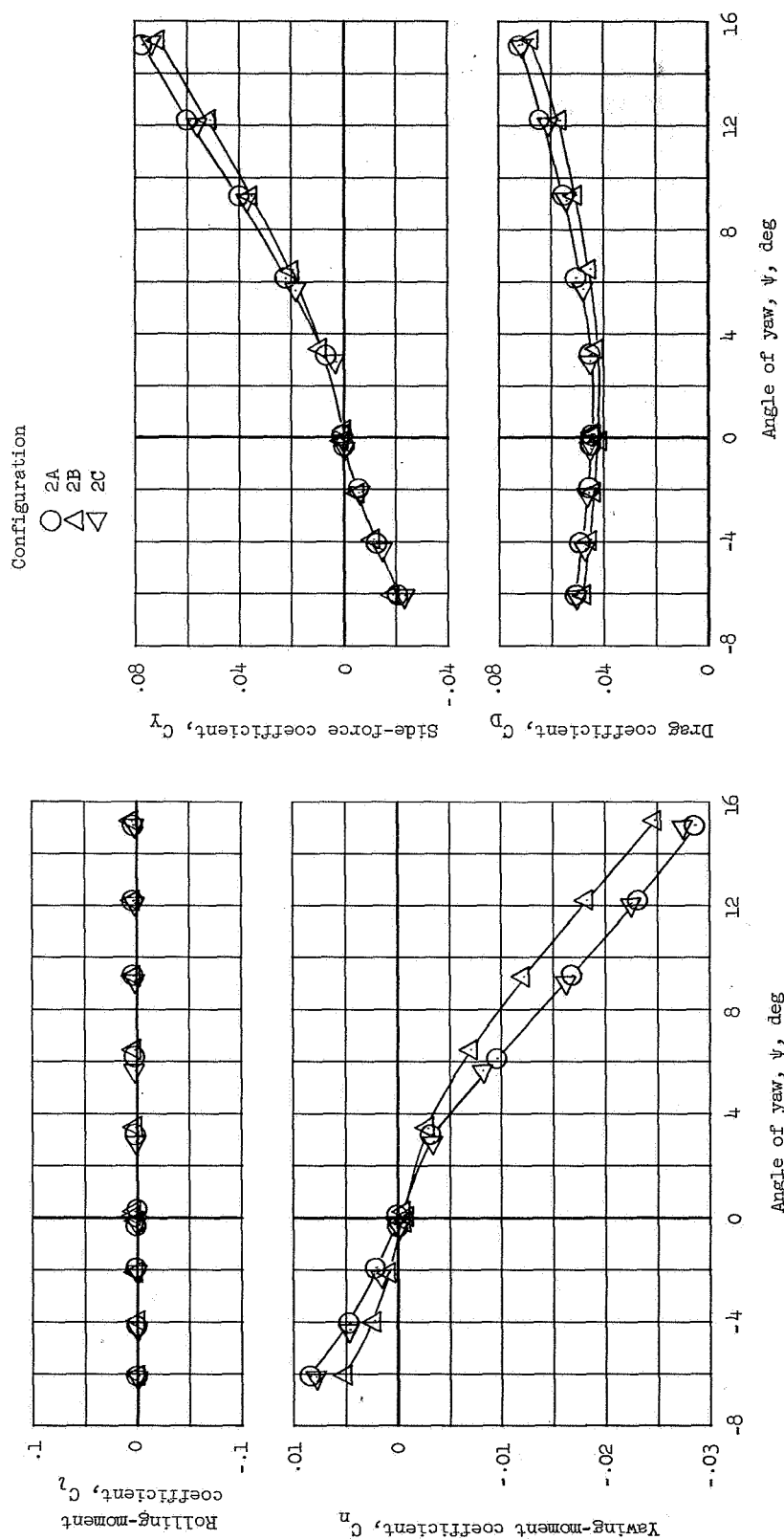
(b) Lateral characteristics.

Figure 6.- Concluded.

32
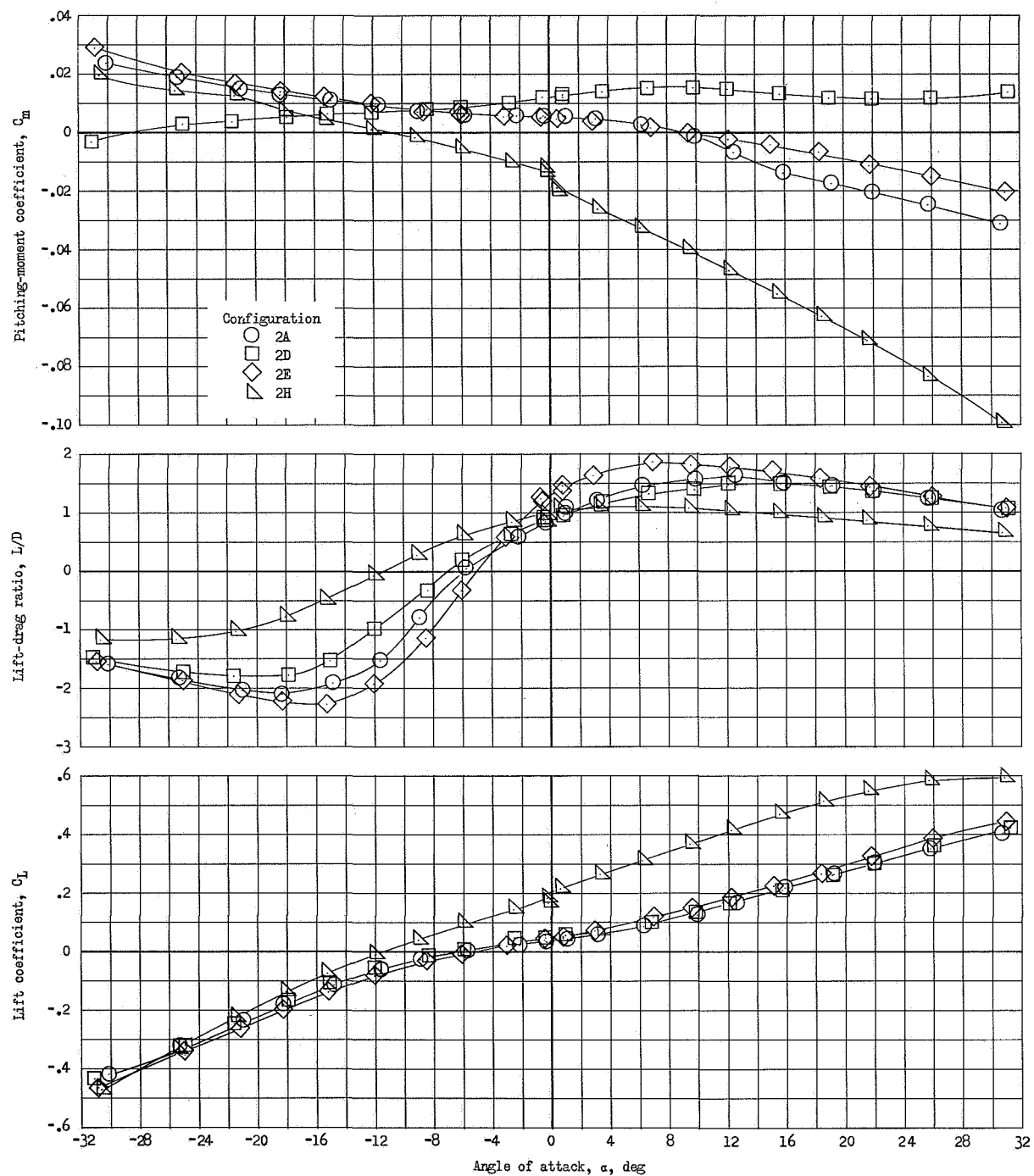
(a) Longitudinal characteristics.

Figure 7.- Effect of variations in planform on static aerodynamic characteristics of basic flat-top conoidal lifting body.
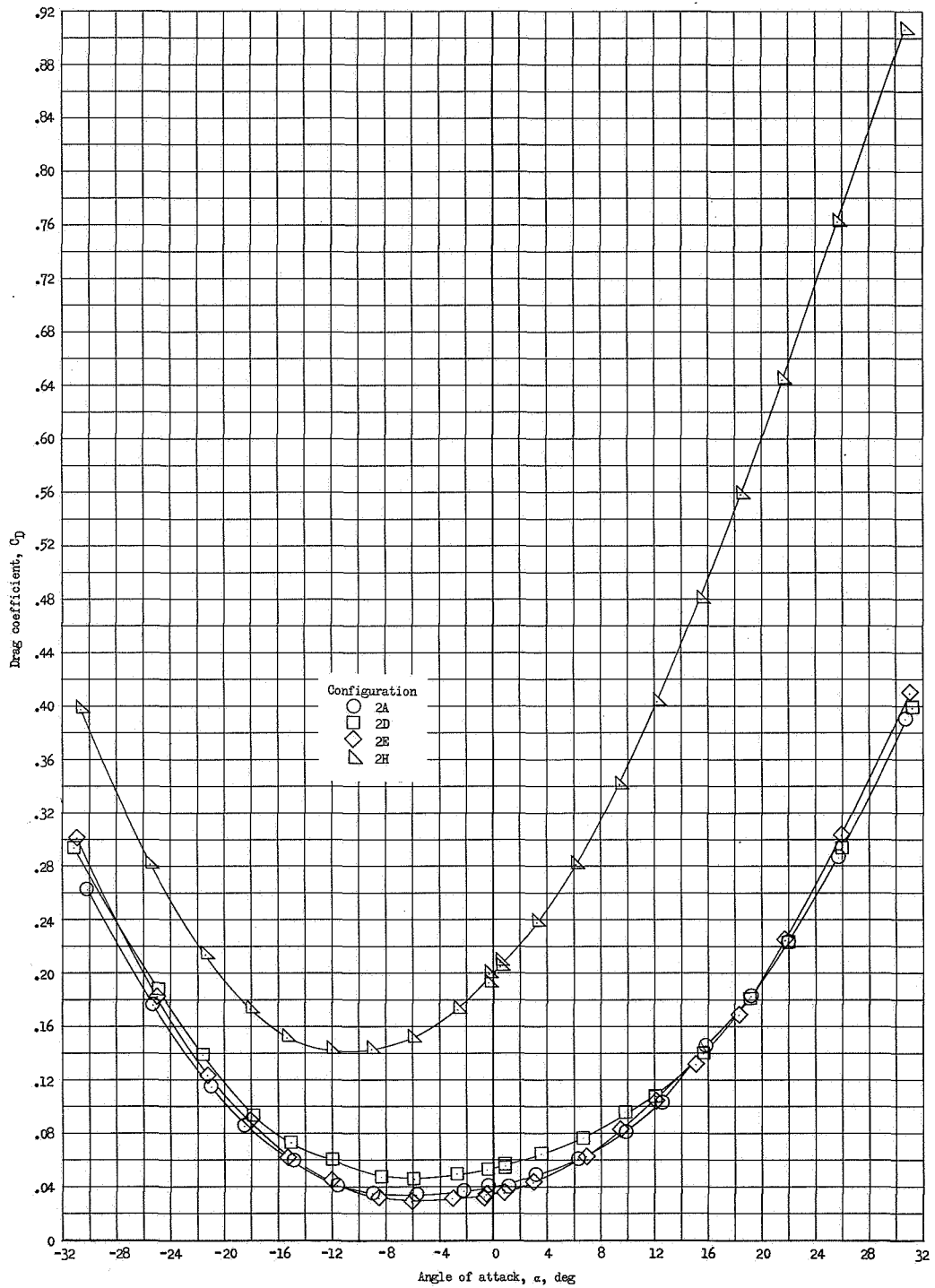
(a) Concluded.

Figure 7.- Continued.
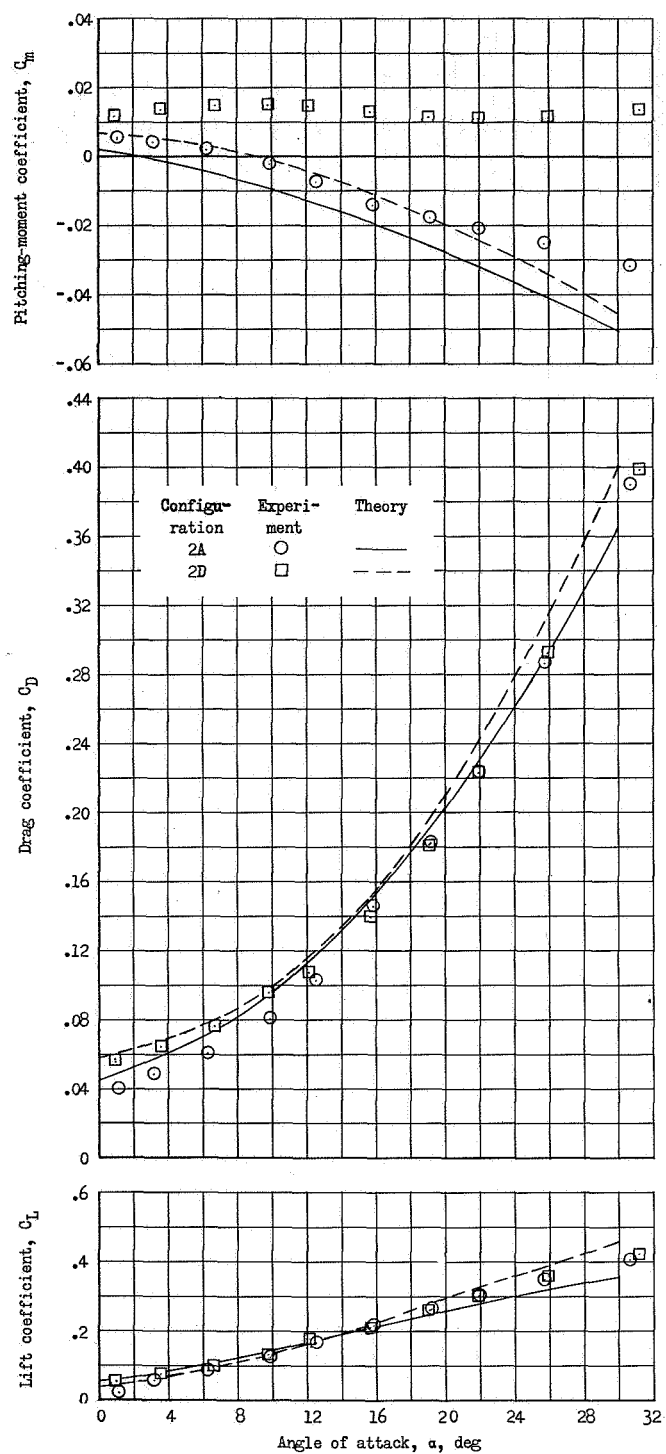
(b) Effect of planform variation. Comparison of data and theory for configurations 2A and 2D.

Figure 7.- Continued.
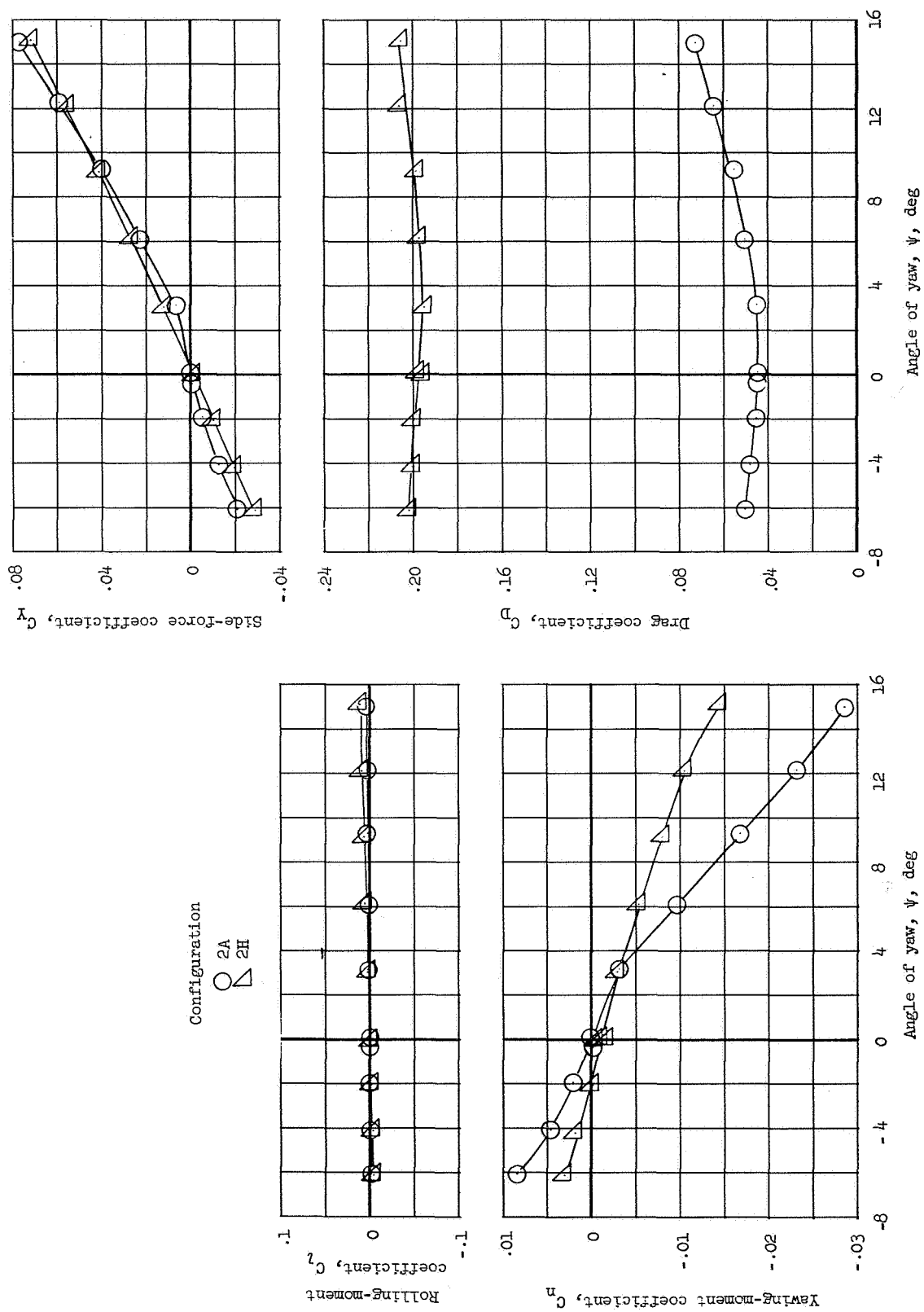
(c) Lateral characteristics.

Figure 7.- Concluded.
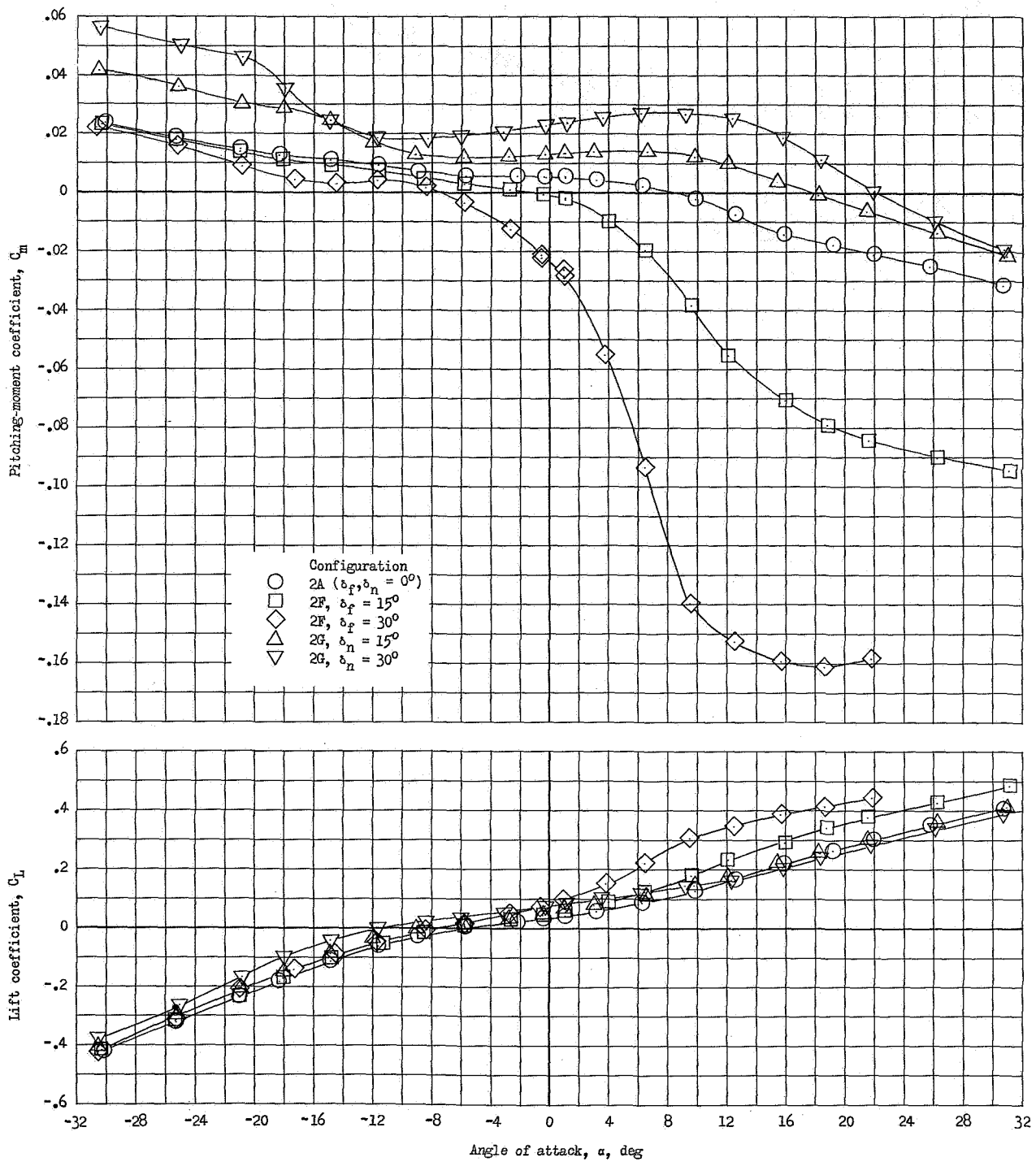
(a) Experimental data.

Figure 8.- Aerodynamic characteristics of flat-top conoidal pitch-control models.

Configuration
○ 2A ($\delta_f, \delta_n = 0°$)
□ 2F, $\delta_f = 15°$
◇ 2F, $\delta_f = 30°$
△ 2G, $\delta_n = 15°$
▽ 2G, $\delta_n = 30°$
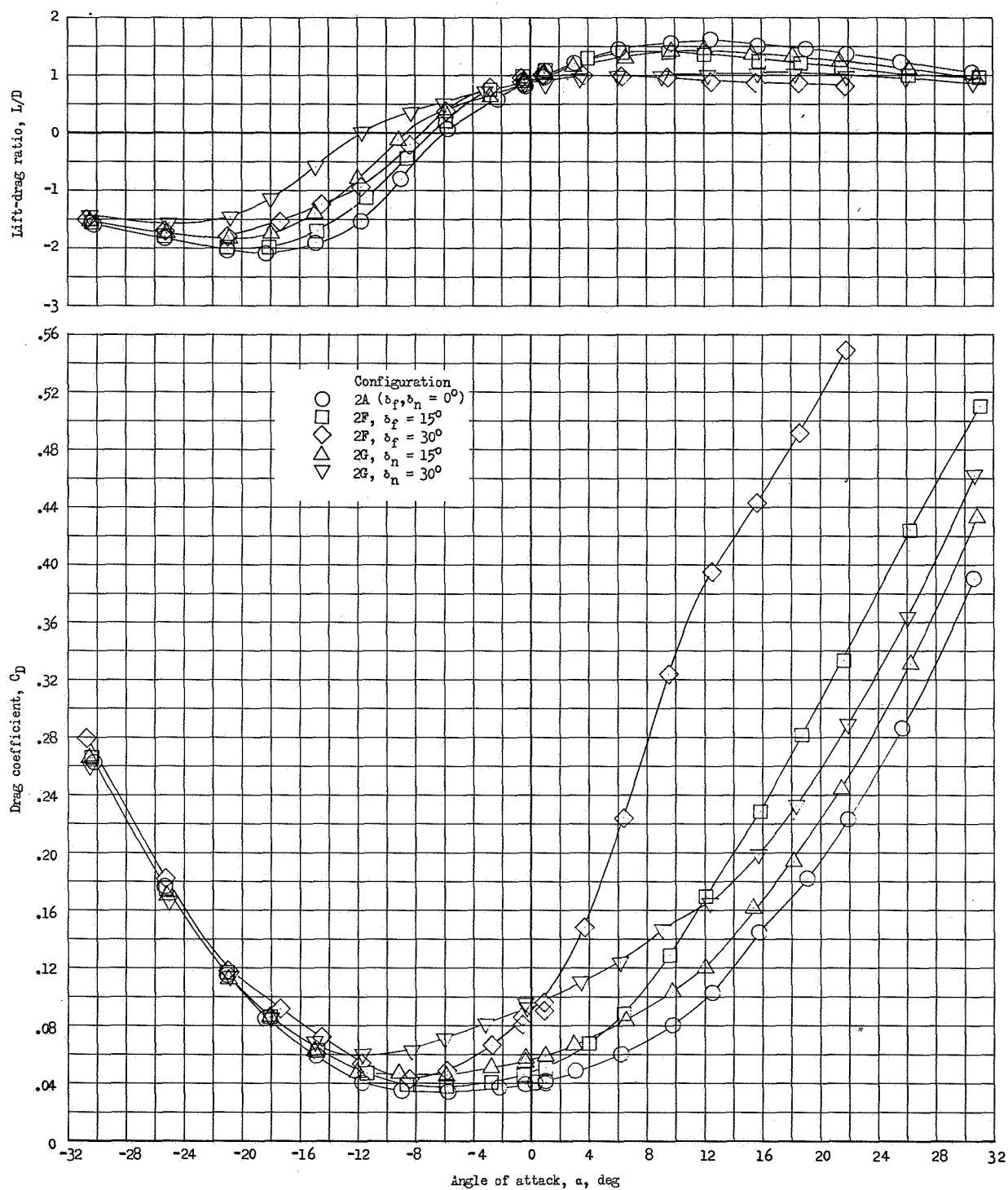
(a) Concluded.

Figure 8.- Continued.

Configuration Experiment Theory

2A ($\delta_n = 0°$)   O   ———
2G, $\delta_n = 15°$ △   ———
2G, $\delta_n = 30°$ ▽   ———
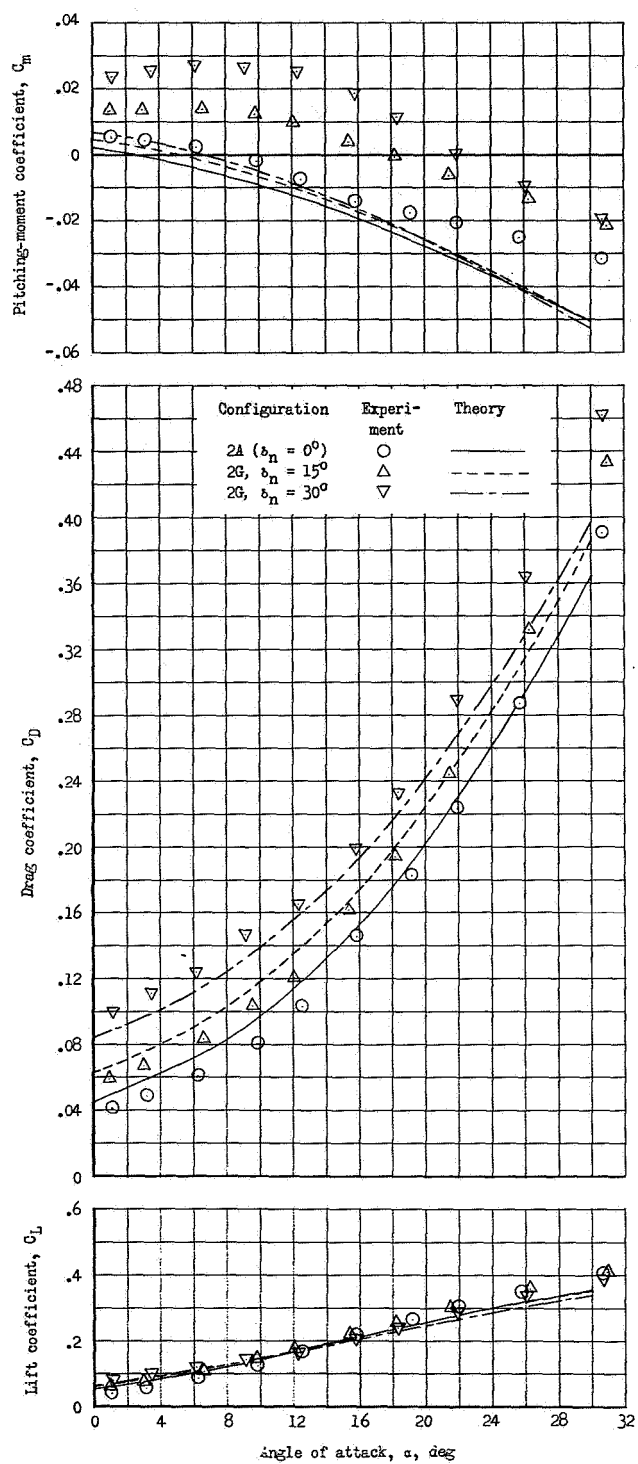
(b) Comparison of data and theory for forward pitch-control configuration 2G.

Figure 8.- Concluded.

Configuration
○ 3A
□ 3B
◇ 3C
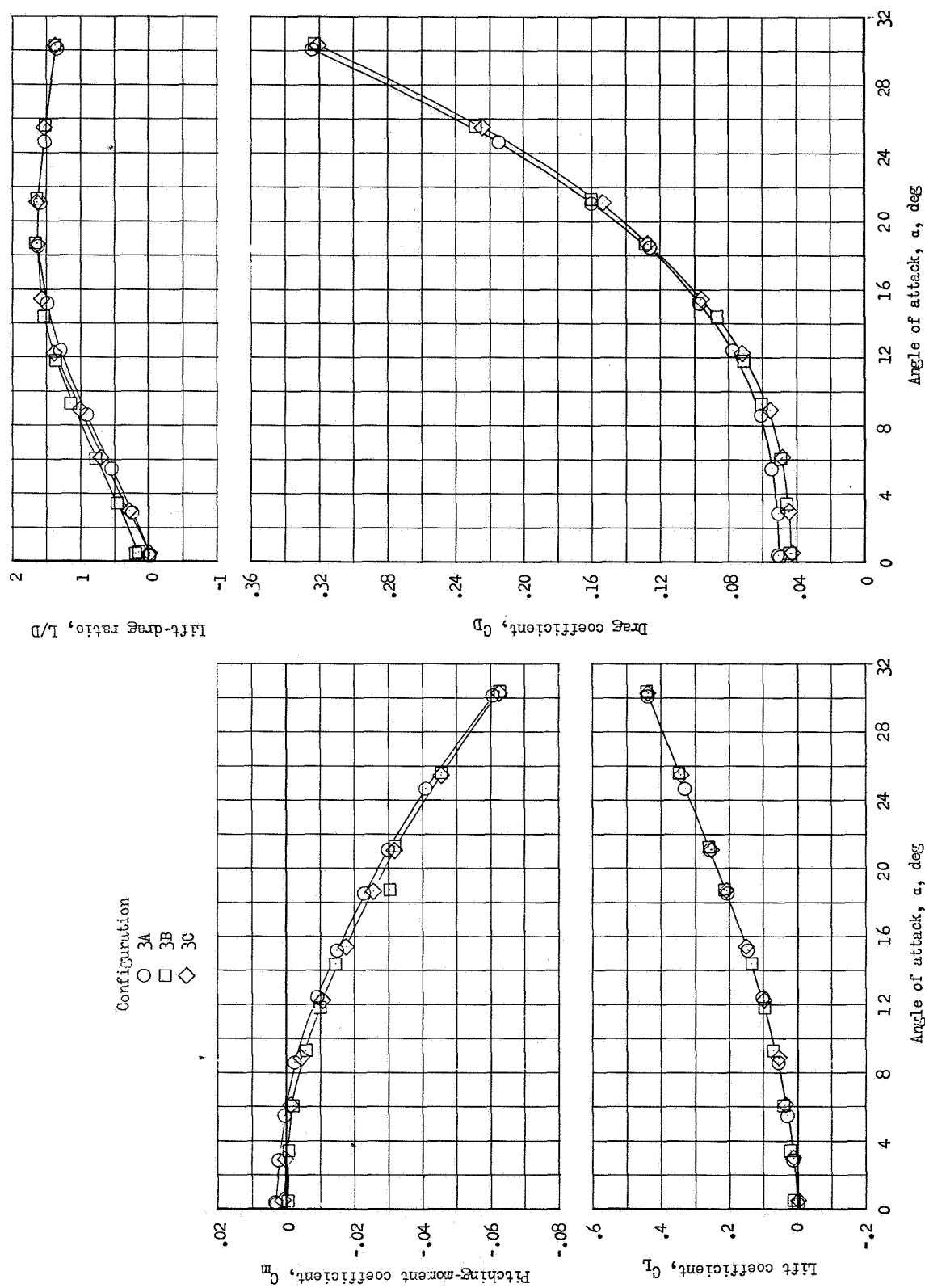
(a) Aerodynamic characteristics.

Figure 9.- Aerodynamic characteristics of Clark-Y winged configurations.
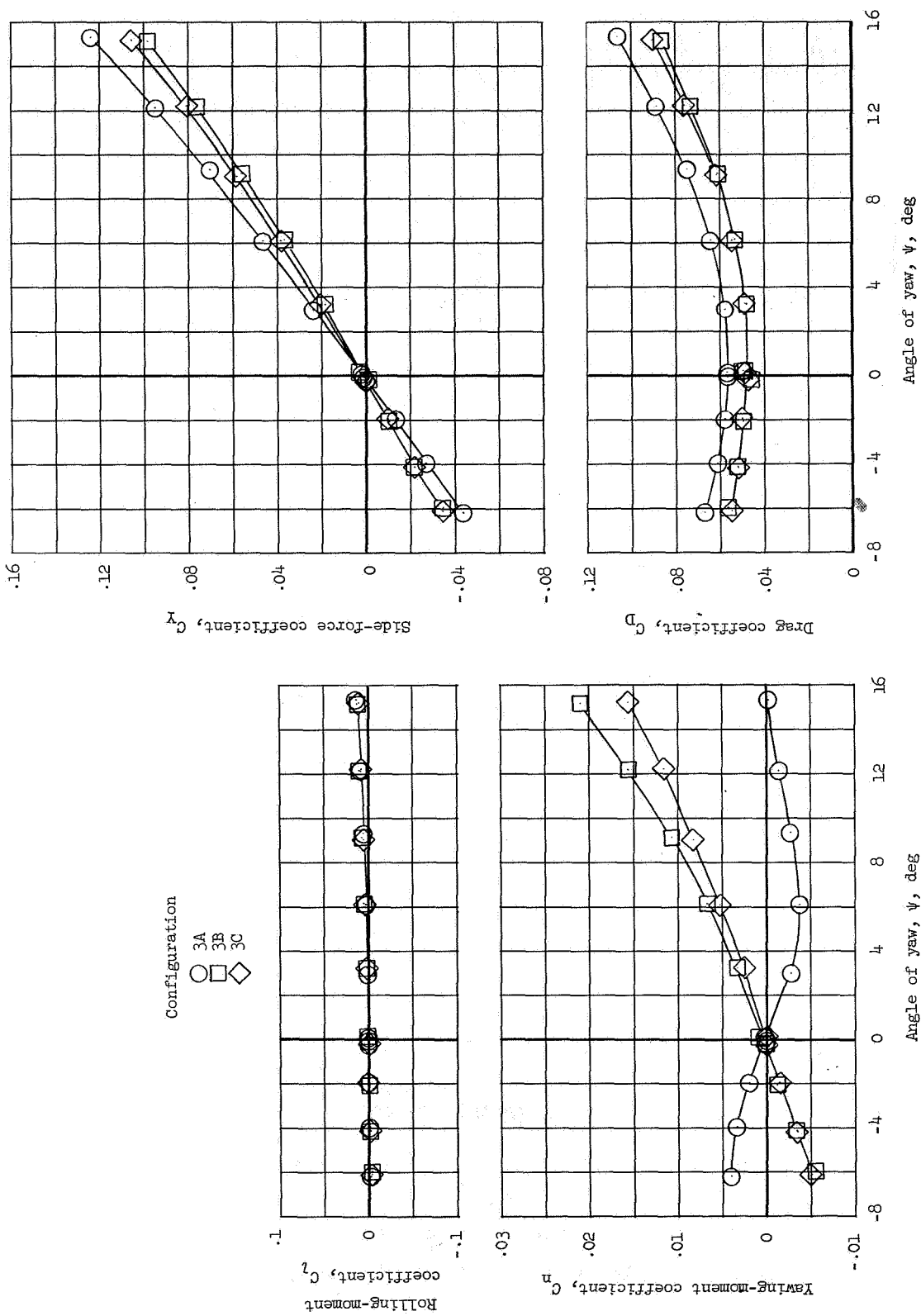
(b) Lateral characteristics.

Figure 9.- Concluded.
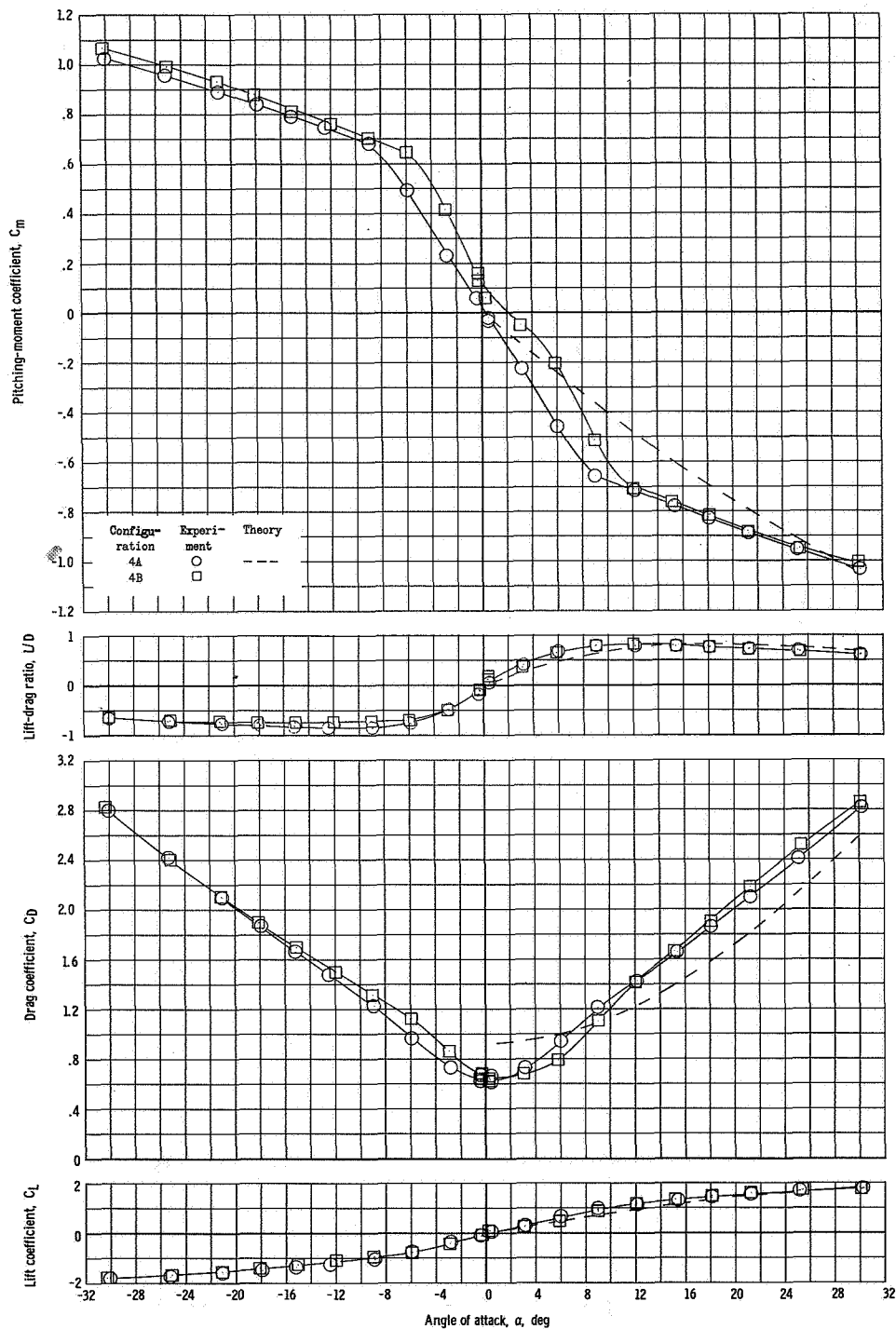
(a) Longitudinal data and Newtonian impact theory.

Figure 10.- Aerodynamic characteristics of cone-flare models.
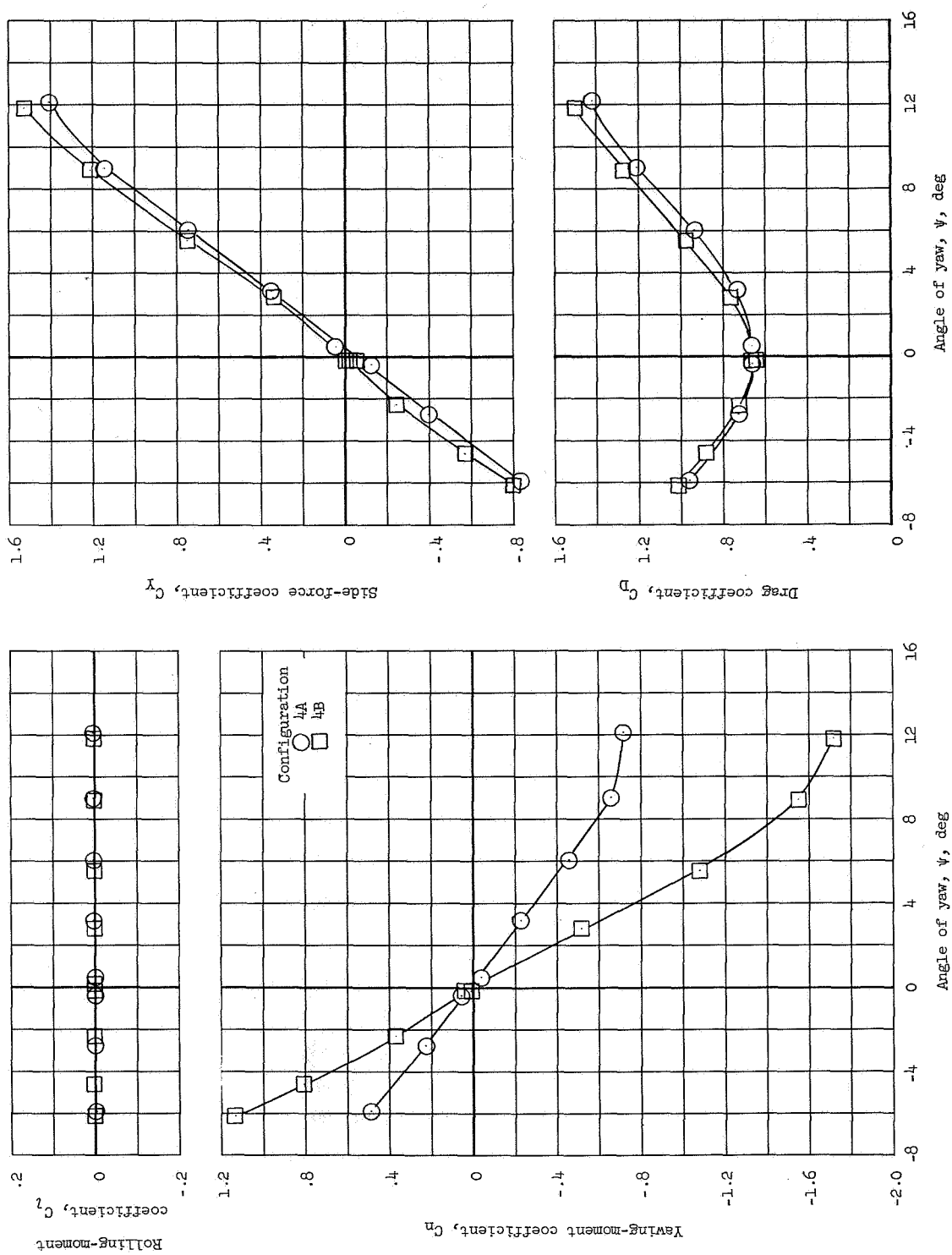
(b) Lateral characteristics.

Figure 10.- Concluded.
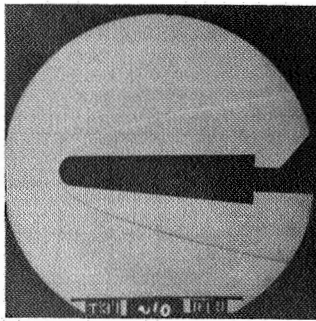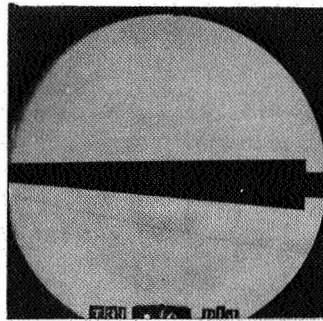
$\alpha = .80^{\circ}$ $\alpha = -.30$
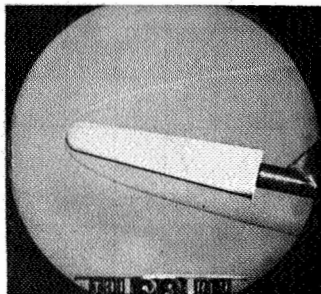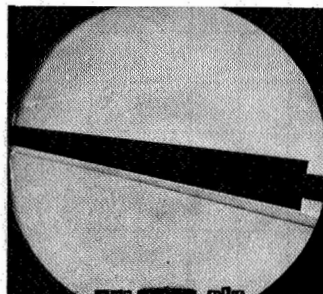
$\alpha = 9.45^{\circ}$ $\alpha = 8.62^{\circ}$
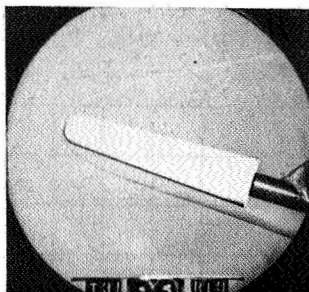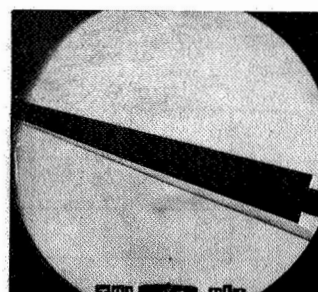
$\alpha = 15.33^{\circ}$ $\alpha = 14.47^{\circ}$
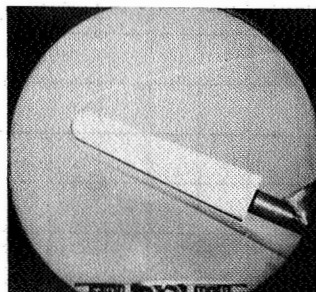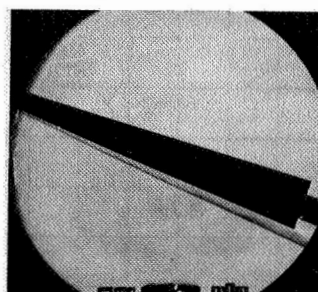
$\alpha = 21.44^{\circ}$ $\alpha = 19.57^{\circ}$

Configuration 1A   Configuration 1E

(a) Conoidal configurations 1A and 1E.   L-64-437

Figure 11.- Selected schlieren photographs of models.
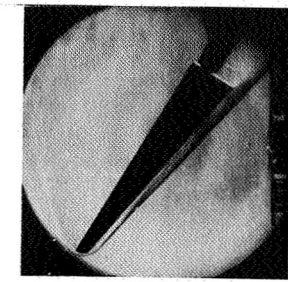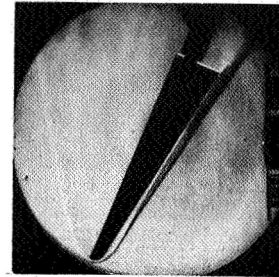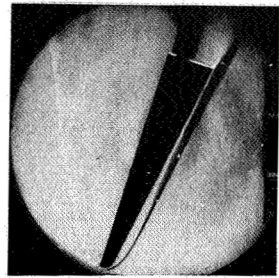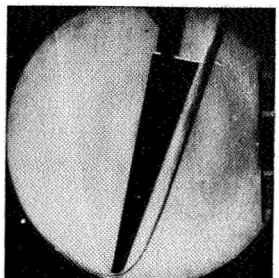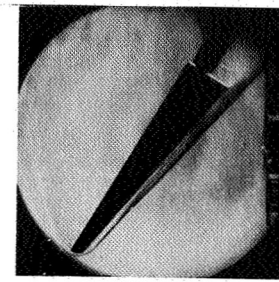
α = 30.65°   α = 21.96°   α = 15.80°   α = 9.81°   α = 1.06°

Configuration 2A

α = 31.20°   α = 21.90°   α = 15.20°   α = 9.76°   α = .88°
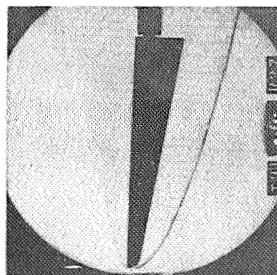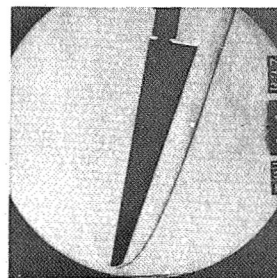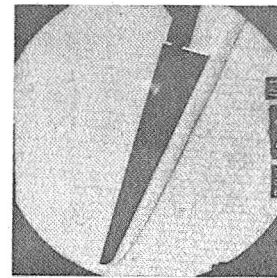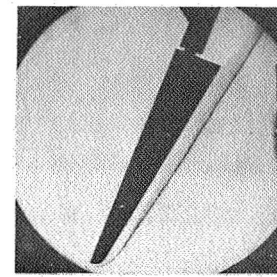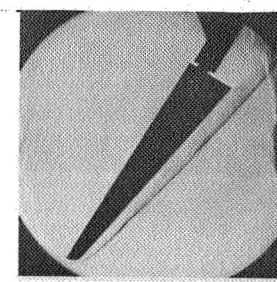
Configuration 2D

L-64-438

(b) Flat-top conoidal configurations 2A and 2D.

Figure 11.- Continued.

$\alpha = 31.08°$

$\alpha = 15.87°$

$\alpha = 15.63°$

$\alpha = -.49°$

Configuration 2F $(\delta_f = 15°)$

$\alpha = -.61°$

$\alpha = -14.81°$

$\alpha = -14.50°$

Configuration 2F $(\delta_f = 30°)$

$\alpha = -30.36°$

$\alpha = -30.69°$
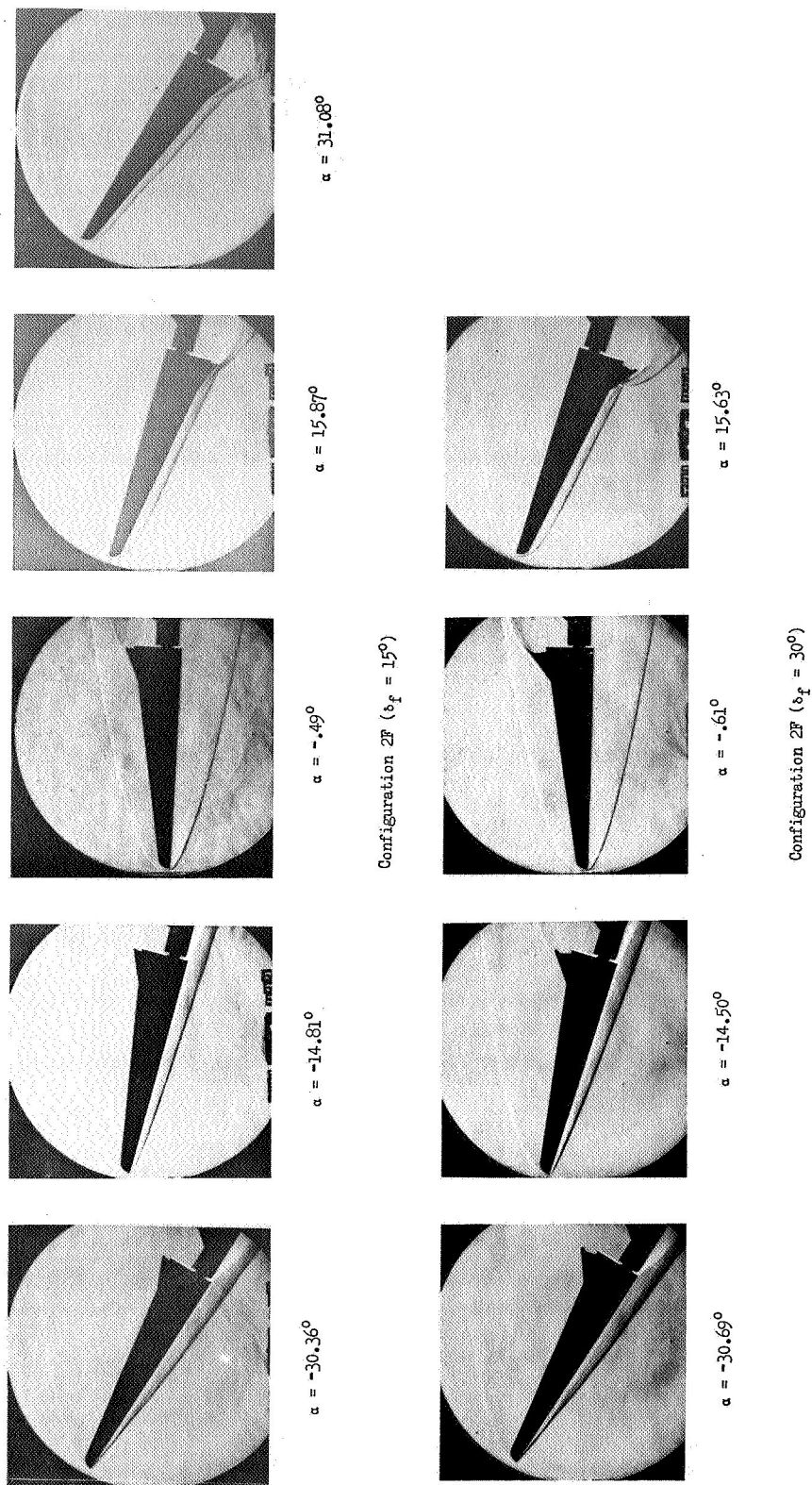
L-64-439

(c) Aft pitch-control configurations 2F $(\delta_f = 15°)$ and 2F $(\delta_f = 30°)$. (Negative angles obtained by inverting model.)

Figure 11.- Continued.

46

$\alpha = 30.93^{\text{o}}$

$\alpha = 15.35^{\text{o}}$

$\alpha = -.40^{\text{o}}$

$\alpha = -14.94^{\text{o}}$

Configuration 2G ($\delta_n = 15^{\text{o}}$)

$\alpha = 30.67^{\text{o}}$

$\alpha = 15.76^{\text{o}}$

$\alpha = -.37^{\text{o}}$

$\alpha = -14.90^{\text{o}}$
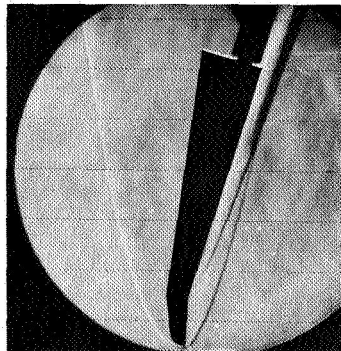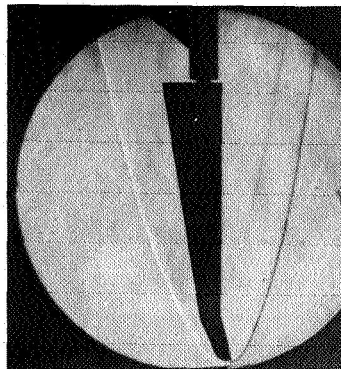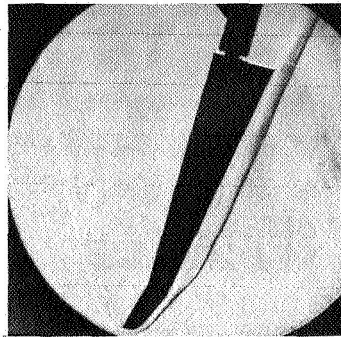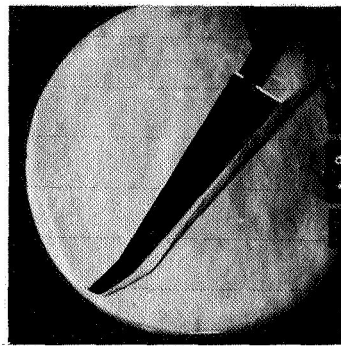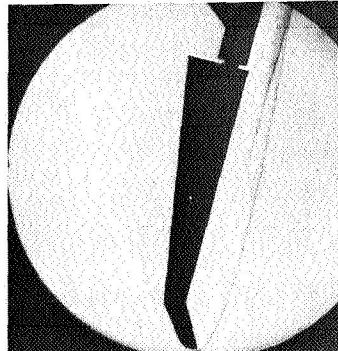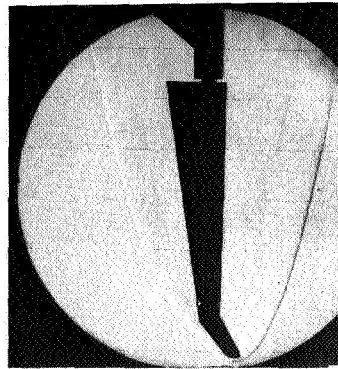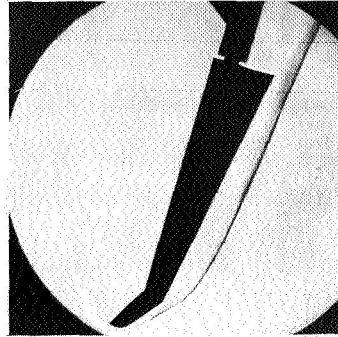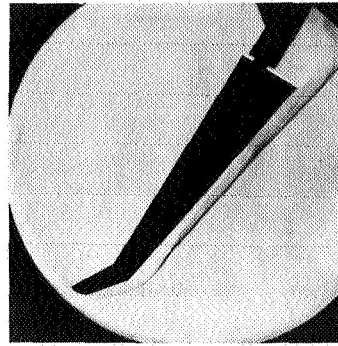
Configuration 2G ($\delta_n = 30^{\text{o}}$)

L-64-440

(d) Forward pitch-control configurations 2G ($\delta_n = 15^{\text{o}}$) and 2G ($\delta_n = 30^{\text{o}}$). (Negative angles obtained by inverting model.)

Figure 11.- Continued.

$\alpha = .36^o$

$\alpha = .48^o$

$\alpha = .52^o$

$\alpha = 30.15^o$

$\alpha = 30.39^o$

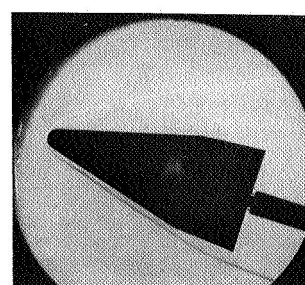$\alpha = 30.32^o$

$\psi = -.22^o$

$\psi = -.015^o$

$\psi = -.25^o$

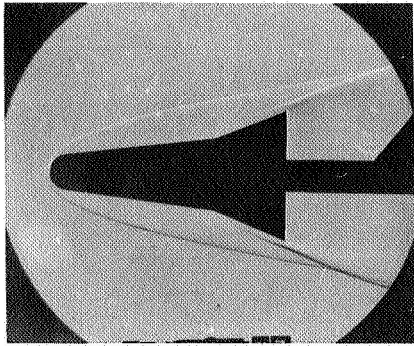$\psi = 15.35^o$
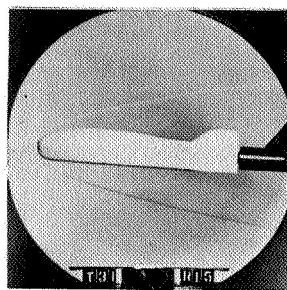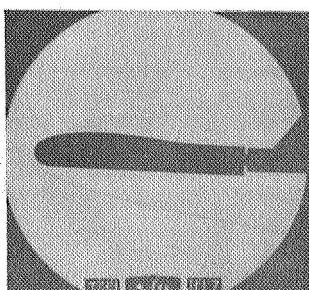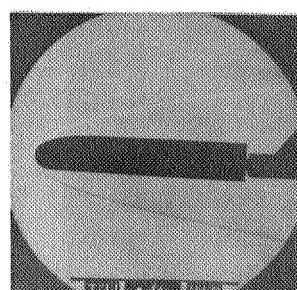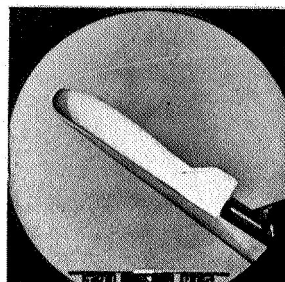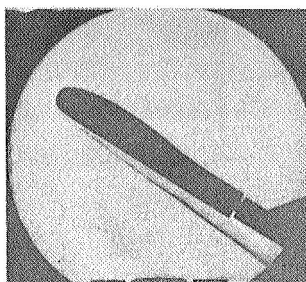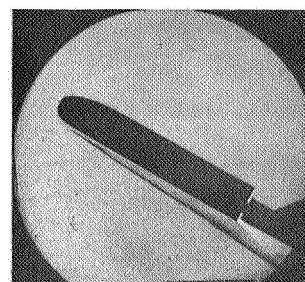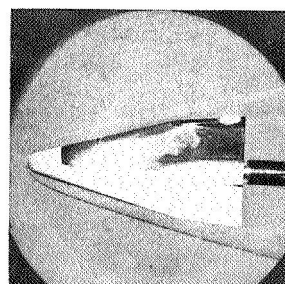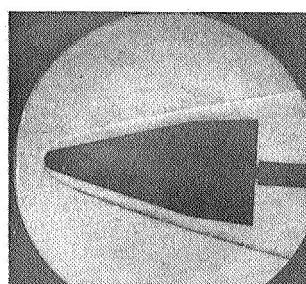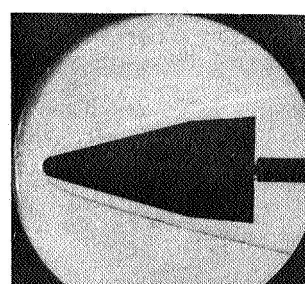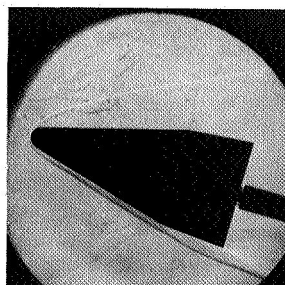
Configuration 3A

$\psi = 15.16^o$
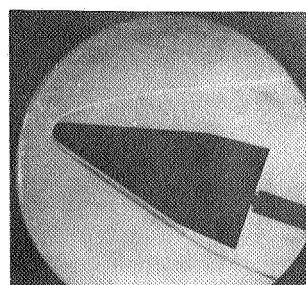
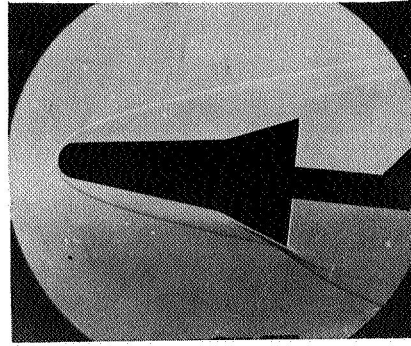Configuration 3B

$\psi = 15.22^o$

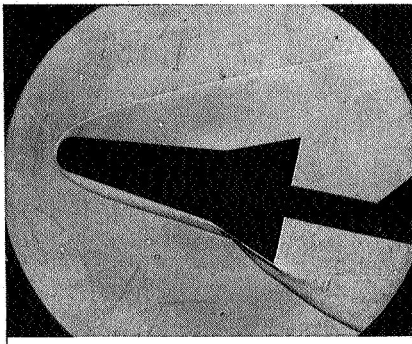Configuration 3C

(e) Clark-Y configurations 3A, 3B, and 3C.

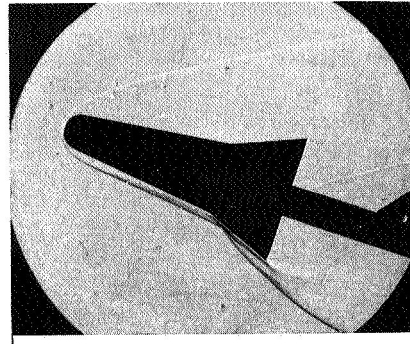Figure 11.- Continued.

L-64-441
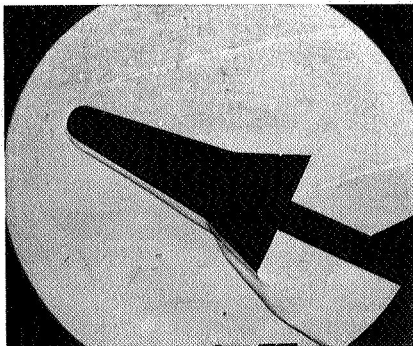
$\alpha = .38^{\circ}$
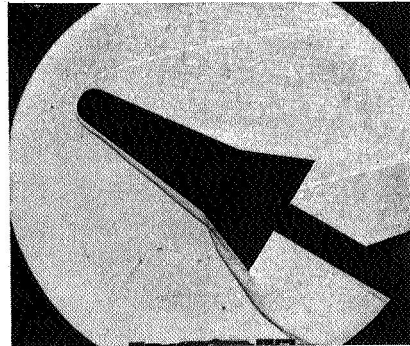
$\alpha = 5.90^{\circ}$

$\alpha = 12.46^{\circ}$

$\alpha = 17.92^{\circ}$

$\alpha = 25.26^{\circ}$

$\alpha = 30.02^{\circ}$

Configuration 4A

(f) Cone-flare configuration 4A.

L-64-442

Figure 11.- Concluded.

NASA SCIENTIFIC AND TECHNICAL PUBLICATIONS

TECHNICAL REPORTS: Scientific and technical information considered important, complete, and a lasting contribution to existing knowledge.

TECHNICAL NOTES: Information less broad in scope but nevertheless of importance as a contribution to existing knowledge.

TECHNICAL MEMORANDUMS: Information receiving limited distribution because of preliminary data, security classification, or other reasons.

CONTRACTOR REPORTS: Technical information generated in connection with a NASA contract or grant and released under NASA auspices.

TECHNICAL TRANSLATIONS: Information published in a foreign language considered to merit NASA distribution in English.

TECHNICAL REPRINTS: Information derived from NASA activities and initially published in the form of journal articles.

SPECIAL PUBLICATIONS: Information derived from or of value to NASA activities but not necessarily reporting the results of individual NASA-programmed scientific efforts. Publications include conference proceedings, monographs, data compilations, handbooks, sourcebooks, and special bibliographies.

Details on the availability of these publications may be obtained from:

SCIENTIFIC AND TECHNICAL INFORMATION DIVISION

NATIONAL AERONAUTICS AND SPACE ADMINISTRATION

Washington, D.C. 20546